Anisotropic tunneling magnetoresistance and tunneling anisotropic magnetoresistance: Spin-orbit coupling in magnetic tunnel junctions

A. Matos-Abiague and J. Fabian

Institute for Theoretical Physics, University of Regensburg, 93040 Regensburg, Germany

(Received 22 July 2008; revised manuscript received 14 January 2009; published 6 April 2009)

The effects of the spin-orbit coupling (SOC) on the tunneling magnetoresistance of ferromagnet/semiconductor/normal-metal tunnel junctions are investigated. Analytical expressions for the tunneling anisotropic magnetoresistance (TAMR) are derived within an approximation in which the dependence of the magnetoresistance on the magnetization orientation in the ferromagnet originates from the interference between Bychkov-Rashba and Dresselhaus SOCs that appear at junction interfaces and in the tunneling region. We also investigate the TAMR effect in ferromagnet/semiconductor/ferromagnet tunnel junctions. The conventional tunneling magnetoresistance (TMR) measures the difference between the magnetoresistance in parallel and antiparallel configurations. We show that in ferromagnet/semiconductor/ferromagnet heterostructures, because of the SOC effects, the conventional TMR becomes anisotropic—we refer to it as the anisotropic tunneling magnetoresistance (ATMR). The ATMR describes the changes in the TMR when the axis along which the parallel and antiparallel configurations are defined is rotated with respect to a crystallographic reference axis. Within the proposed model, depending on the magnetization directions in the ferromagnets, the interplay of Bychkov-Rashba and Dresselhaus SOCs produces differences between the rates of transmitted and reflected spins at the ferromagnet/semiconductor interfaces, which results in an anisotropic local density of states at the Fermi surface and in the TAMR and ATMR effects. Model calculations for Fe/GaAs/Fe tunnel junctions are presented. Finally, based on rather general symmetry considerations, we deduce the form of the magnetoresistance dependence on the absolute orientations of the magnetizations in the ferromagnets.

DOI: 10.1103/PhysRevB.79.155303 PACS number(s): 73.43.Jn, 72.25.Dc, 73.43.Qt

I. INTRODUCTION

The tunneling magnetoresistance (TMR) effect is observed in ferromagnet/insulator/ferromagnet heterojunctions, in which the magnetoresistance exhibits a strong dependence on the relative magnetization directions in the two ferromagnetic layers and on their spin polarizations.[1–6] Because of this peculiarly strong asymmetric behavior of the magnetoresistance, TMR devices find multiple uses ranging from magnetic sensors to magnetic random access memory applications.[4,5]

Beyond the conventional TMR effect, it has been observed that the magnetoresistance in magnetic tunnel junctions (MTJs) may also depend on the orientation of the magnetizations in the ferromagnetic leads with respect to the crystallographic axes.[7–12] This phenomenon is called the tunneling anisotropic magnetoresistance (TAMR) effect. It is remarkable that TAMR is present even in MTJs in which only one of the electrodes is magnetic and the conventional TMR is absent.[9,13] Thus, in contrast to the conventional TMR-based devices, which require two magnetic layers for their operation, TAMR-based devices can operate with a single magnetic lead, opening new possibilities and functionalities for the operation of spintronic devices. The TAMR may also affect the spin injection from a ferromagnet into a nonmagnetic semiconductor. Therefore, in order to correctly interpret the results of spin injection experiments in a spin-valve configuration, it is essential to understand the nature, properties, and origin of the TAMR effect.

Depending on the specific configuration considered, different authors have used different expressions for quantifying TAMR (see, for example, Refs. 6, 9, 12, 14, and 15). However, the phenomenon is indistinctly referred to as TAMR. In order to clearly distinguish between these different definitions, we classify them in what we call here *out-of-plane* and *in-plane* TAMR. The out-of-plane TAMR in a MTJ with a single magnetic layer refers to the changes in the tunneling magnetoresistance when the magnetization is rotated within a plane perpendicular to the ferromagnetic layer. The situation is illustrated in Fig. 1(a), where the unit vector $\mathbf{n}$ denotes the magnetization direction measured with respect to the film normal direction and R is the tunneling magnetoresistance. The reference crystallographic axis denoted by $[x]$ and the film normal direction define the plane in which the magnetization is rotated. On the other hand, the in-plane TAMR [see Fig. 1(b)] refers to the changes in the tunneling magnetoresistance when the in-plane magnetization direction $\mathbf{n}$, defined with respect to a fixed reference axis $[x]$, is rotated in the plane of the ferromagnetic layer. In both cases, the out-of-plane and the in-plane, the TAMR coefficient is determined by

$$\mathrm{TAMR}_{[x]}(\phi)=\frac{R(\phi)-R(0)}{R(0)}. \tag{1}$$

While this definition is *formally* the same for both the out-of-plane and in-plane configurations, the meaning of the angle ϕ is different in each case. In fact, the two configurations correspond to different physical situations. While in the out-of-plane configuration the tunneling magnetoresistance changes due to the different orientations of the magnetization with respect to the direction of the current flow, the situation becomes more subtle in the in-plane configuration, where the

 ©2009 The American Physical Society

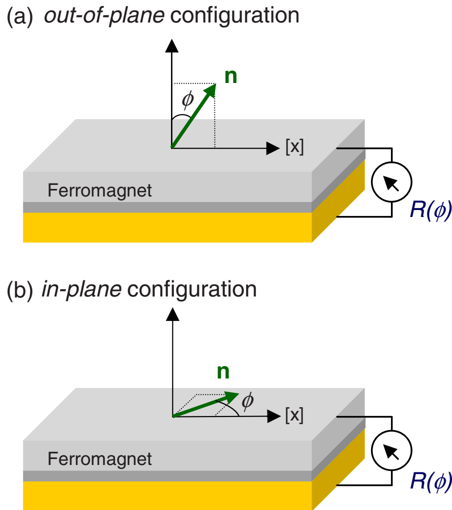

FIG. 1. (Color online) Schematics of the configurations used for measuring the TAMR in MTJs in which one of the leads is ferromagnetic. (a) Out-of-plane configuration. (b) In-plane configuration. The vector $\mathbf{n}$ indicates the magnetization orientation, while $[x]$ refers to a reference crystallographic axis. The tunneling magnetoresistance $R(\phi)$ depends on the magnetization direction specified by the angle ϕ.

magnetization remains always perpendicular to the current direction.

The TAMR is also present in MTJs with two ferromagnetic leads. In such systems, the tunneling magnetoresistance $R(\theta,\phi)$ depends on the magnetization directions, $\mathbf{n}_l$ and $\mathbf{n}_r$, of the ferromagnetic layers (see Fig. 2). In the conventional TMR, the tunneling magnetoresistance depends only on the relative directions (i.e., R is only a function of θ). In the TAMR, however, the tunneling magnetoresistance depends

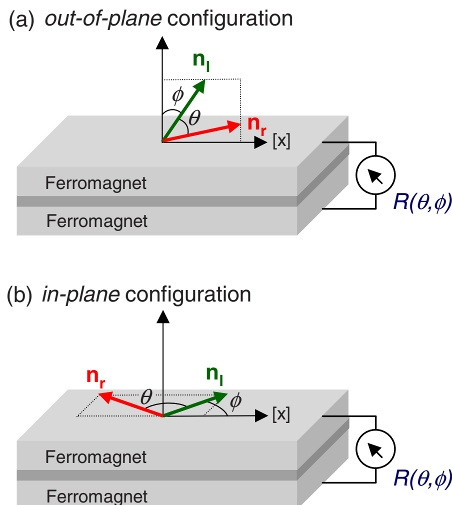

FIG. 2. (Color online) Schematics of the configurations used for measuring the TAMR in MTJs in which both leads are ferromagnetic. (a) Out-of-plane configuration. (b) In-plane configuration. The vectors $\mathbf{n}_l$ and $\mathbf{n}_r$ determine the magnetization orientation in each of the leads and $[x]$ denotes a reference crystallographic axis. The tunneling magnetoresistance $R(\theta,\phi)$ depends on the absolute magnetization directions $\mathbf{n}_l$ and $\mathbf{n}_r$.

on the magnetization directions relative to the crystallographic axes (i.e., R becomes a function of both θ and ϕ). In the out-of-plane configuration the magnetizations $\mathbf{n}_l$ and $\mathbf{n}_r$ of the corresponding ferromagnetic leads are rotated in the plane defined by the reference axis $[x]$ and the normal to the layers direction [see Fig. 2(a)], while in the in-plane configuration $\mathbf{n}_l$ and $\mathbf{n}_r$ are rotated in the plane of the layers [see Fig. 2(a)]. The definition of the TAMR in Eq. (1) can be generalized to the case of MTJs with two ferromagnetic leads as follows:

$$\mathrm{TAMR}_{[x]}(\theta,\phi) = \frac{R(\theta,\phi) - R(\theta,0)}{R(\theta,0)}. \qquad (2)$$

Here as in Eq. (1) the meaning of the angles θ and ϕ depends on the specific configuration considered. Note also that there is no ambiguity in the notation used in Eqs. (1) and (2): the number of arguments in the TAMR coefficient [one argument (ϕ) in the case of MTJs with a single magnetic electrode and two arguments (θ and ϕ) in the case of MTJs with two magnetic leads] eliminates any possible confusion between the two cases.

Another interesting effect may emerge in MTJs with two magnetic leads when the conventional TMR becomes anisotropic. The conventional TMR is defined as

$$\mathrm{TMR} = \frac{R_{\mathrm{AP}} - R_{\mathrm{P}}}{R_{\mathrm{P}}}, \qquad (3)$$

where R_{P} (R_{AP}) is the magnetoresistance measured when the magnetization of the ferromagnetic layers are parallel (P) [antiparallel (AP)]. Allowing for a dependence of the tunneling magnetoresistance on the specific axis along which the parallel and antiparallel configurations are defined, the anisotropic tunneling magnetoresistance (ATMR) can be defined as

$$\mathrm{ATMR}_{[x]}(\phi) = \frac{R_{\mathrm{AP}}(\phi) - R_{\mathrm{P}}(\phi)}{R_{\mathrm{P}}(\phi)}, \qquad (4)$$

where the resistances in parallel and antiparallel configurations are, respectively, $R_{\mathrm{P}}(\phi)=R(0,\phi)$ and $R_{\mathrm{AP}}(\phi)=R(\pi,\phi)$ [here we have use the same notation for the resistance $R(\theta,\phi)$ as in Fig. 2].

A summary of the abbreviations used throughout the paper is given in Table I.

Most of the early experiments on the magnetization direction dependence of the tunneling magnetoresistance were performed in MTJs with GaMnAs ferromagnetic leads. The in-plane ATMR was experimentally observed in GaMnAs/AlAs/GaMnAs tunnel junctions,[7,8] where in-plane ATMR ratios $\mathrm{ATMR}_{[100]}(0)\approx 75\%$ and $\mathrm{ATMR}_{[100]}(-\pi/4)\approx 30\%$ were found [here we have used the notations introduced in Eqs. (2) and (4)]. A similar but larger effect in GaMnAs/GaAs/GaMnA heterostructures was reported in Ref. 16. The first experimental observation of the TAMR in MTJs with a single magnetic layer was done in (Ga,Mn)As/AlOx/Au heterojunctions, in which an in-plane TAMR ratio of about $\mathrm{TAMR}_{[110]}(\pi/2)\approx 2.7\%$ was found.[9] Theoretical investigations considering the out-of-plane[12,17] and in-plane[17] configurations in GaMnAs based MTJs in which both electrodes

TABLE I. Summary of used abbreviations sorted by alphabetic order.

ALDOS	Anisotropic local density of states
ATMR	Anisotropic tunneling magnetoresistance
DDFM	Dirac-delta function model
F	Ferromagnet
LDOS	Local density of states
MTJ	Magnetic tunnel junction
NM	Normal metal
S	Semiconductor
SOC	Spin-orbit coupling
SOCF	Spin-orbit coupling field
SSOM	Slonczewski spin-orbit model
TAMR	Tunneling anisotropic magnetoresistance
TASP	Tunneling anisotropic spin polarization
TMR	Tunneling magnetoresistance

are ferromagnetic have also been reported. Experimentally, tunnel junctions such as (Ga,Mn)As/GaAs/(Ga,Mn)As and (Ga,Mn)As/ZnSe/(Ga,Mn)As have been used for measuring the in-plane TAMR.[10,11] In the case of (Ga,Mn)As/ZnSe/(Ga,Mn)As, the in-plane TAMR ratio $\mathrm{TAMR}_{[110]}(0,\pi/2)$ was found to decrease with increasing temperature, from about 10% at 2 K to 8.5% at 20 K.[11] This temperature dependence of the in-plane TAMR is more dramatic in the case of (Ga,Mn)As/GaAs/(Ga,Mn)As, for which a TAMR ratio of the order of a few hundred percent at 4 K was amplified to 150 000% at 1.7 K.[10] This huge amplification of the in-plane TAMR was suggested to originate from the opening of the Efros-Shklovskii gap[18] at the Fermi energy when crossing the metal-insulator transition.[10] Measurements of the TAMR in p^+-(Ga,Mn)As/n^+-GaAs Esaki diode devices have also been reported.[19,20] In addition to the investigations involving vertical tunneling devices the TAMR has also been studied in break junctions,[21,22] nanoconstrictions,[20,23] and nanocontacts.[24]

Beyond the area of currently low Curie temperature ferromagnetic semiconductors, the TAMR has recently been investigated both theoretically and experimentally in tunnel junctions such as CoFe/MgO/CoFe and CoFe/Al_2O_3/CoFe,[25] Fe/GaAs/Au,[6,13] and multilayer-(Co/Pt)/AlO_x/Pt structures.[15] Experimental investigations in Co/AlO_x/Au (Ref. 26) and theoretical calculations in Fe/MgO/Fe,[14] Fe(001)/vacuum/bcc-Cu(001),[27] CoPt structures,[28] and in layered bimetallic nanostructures of the type Mn/W(001)[29] have also been reported.

In Table II we show some of the previous investigations in MTJs with metallic ferromagnets specifying the used configuration.

Role of spin-orbit coupling

Most of the theoretical investigations have been devoted to the out-of-plane TAMR in MTJs with isolating barriers.[9,14,15,25,27] For the case of asymmetric structures the Bychkov-Rashba-type SOC due to the strong electric field across the ferromagnet/insulator interface has been identified as being the responsible mechanism for the out-of-plane TAMR. An intuitive simple picture of the role of the SOC is explained as follows. Consider, for simplicity, a MTJ with a single ferromagnetic lead, as the one sketched in Fig. 1(a). The potential gradient along the growth direction generates the effective Bychkov-Rashba spin-orbit coupling (SOC) field (SOCF),

$$\mathbf{w}_{\mathrm{BR}} = (-\alpha k_y, \alpha k_x, 0), \tag{5}$$

where α is the Bychkov-Rashba SOC parameter and $\mathbf{k}_\parallel = (k_x, k_y)$ is the wave vector in the plane of the layers. The observation that $\mathbf{w}_{\mathrm{BR}}$ lies in a plane parallel to the layers suggests that the situation in which the magnetization direction $\mathbf{n}$ and the Bychkov-Rashba SOCF $\mathbf{w}_{\mathrm{BR}}$ are coplanar (i.e., when $\phi=\pi/2$) differs from the case in which $\phi \neq \pi/2$ [see Fig. 1(a)]. In fact, the effective Bychkov-Rashba SOC shifts the electron energy by[27]

TABLE II. Some typical theoretical (theor) and experimental (expt) values of the TAMR and ATMR in MTJs with metallic ferromagnets for different configurations. Note that the notation used here for the TAMR and ATMR [see Eqs. (1)–(4)] may differ from the ones in the original references.

System	Reported quantities	Typical values	Ref.
Fe(001)/vacuum/Cu(001)	out-of-plane $\mathrm{TAMR}_{[100]}(\phi=\pi/2)$	20%[a] (theor)	27
	in-plane $\mathrm{TAMR}_{[110]}(\phi=-\pi/4)$	10%[a] (theor)	
Fe/GaAs/Au	in-plane $\mathrm{TAMR}_{[110]}(\phi)$	−0.4%[b] (expt and theor)	6 and 13
CoFe/MgO/CoFe	out-of-plane differential conductance		25
CoFe/Al_2O_3/CoFe			
(Co/Pt)/AlO_x/Pt	out-of-plane $\mathrm{TAMR}_{[x]}(\phi)$	−12.5%[c] (expt)	15
Fe/FeO/MgO/FeO/Fe	out-of-plane $\mathrm{ATMR}_{[100]}(\phi=0)$	4205% (theor)	14
	out-of-plane $\mathrm{ATMR}_{[100]}(\phi=\pi/2)$	2956% (theor)	
	out-of-plane $\mathrm{TAMR}_{[100]}(\theta=0,\phi=\pi/2)$	44% (theor)	

[a]Taken at a bias voltage of about −50 mV.
[b]Taken at $\phi=\pi/2$ and bias voltage −90 mV.
[c]Taken at $\phi=\pi/2$ and bias voltage −5 mV.

$$\Delta E_{\uparrow,\downarrow} = \pm \mathbf{w}_{\mathrm{BR}} \cdot \mathbf{n}, \tag{6}$$

where ↑ and ↓ refer to the up- and down-spin channels, respectively. In this way, the energy bands become anisotropic with respect to the magnetization direction **n**. For example, $\Delta E(\mathbf{k}_\parallel)$ vanishes when **n** is normal to the ferromagnetic layer [this corresponds to $\phi=0,\pi$ in Fig. 1(a)], while at nonvanishing $\mathbf{k}_\parallel$, $\Delta E(\mathbf{k}_\parallel)$ remains finite for any other value of ϕ. The final outcome is a ϕ-dependent tunneling magnetoresistance. Furthermore, from Eq. (6) [see also Fig. 1(a)] it follows that the situations at ϕ, $-\phi$, and $\phi+\pi$ are physically equivalent but differ from the case at $\phi+\pi/2$. This implies that the tunneling magnetoresistance must obey the relations $R(\phi) = R(-\phi) = R(\phi+\pi) \neq R(\phi+\pi/2)$, i.e., the tunneling magnetoresistance exhibits a twofold symmetric anisotropy as a function of ϕ. The twofold symmetry of the out-of-plane TAMR has been experimentally observed.[15,25]

Recent experimental investigations of the in-plane TAMR in MTJs with a single ferromagnetic lead have revealed that similarly to the out-of-plane, the in-plane TAMR also exhibits a twofold symmetry[9,13,15] as a function of ϕ (recall, however, that the meaning of the angle ϕ is different for the two configurations, as schematically shown in Fig. 1). One may naively think that, as for the out-of-plane TAMR, the twofold symmetry of the in-plane TAMR originates from the Bychkov-Rashba SOC. However, a simple symmetry analysis shows that in the case of the in-plane TAMR the linear Bychkov-Rashba SOC alone is not sufficient for generating a twofold symmetry. The main observation here is that in such a case the effective Bychkov-Rashba SOCF is invariant under in-plane rotations [see Fig. 4(b)]. Therefore, the orientation of the Bychkov-Rashba SOC vector field relative to the in-plane magnetization is independent of ϕ, and no anisotropy is obtained. The situation may be different if higher orders of the Bychkov-Rashba SOC become relevant. In such a case the C_{4v} symmetry of this SOCF will lead to a fourfold symmetric in-plane TAMR.

In order to explain the twofold symmetry of the in-plane TAMR experimentally observed in (Ga,Mn)As/AlOx/Au heterojunctions the existence of an uniaxial strain was assumed.[9] Surprisingly, recent experiments have shown that in epitaxial Fe/GaAs/Au tunnel junctions the in-plane TAMR exhibits also a twofold symmetry.[13] Because of the high quality matching at the epitaxial Fe/GaAs interface strain effects are unlikely to play a sizable role. What is then the mechanism leading to the observed twofold symmetry of the in-plane TAMR in Fe/GaAs/Au tunnel junctions? We have proposed (see Refs. 6 and 13) that the twofold symmetry of the in-plane TAMR originates from the interference of the Bychkov-Rashba and Dresselhaus SOCs. The presence of GaAs, a zinc-blende semiconductor, as the barrier material plays here a decisive role. Zinc-blende semiconductors are noncentrosymmetric. Therefore, the so-called Dresselhaus SOC, which originates from the bulk inversion asymmetry (BIA) of the semiconductor is *intrinsically* present in such materials. Thus, although the Bychkov-Rashba-type SOC is present in asymmetric MTJs, the Dresselhaus SOC may or not be present, in dependence on the symmetry of the constituent materials. This produces qualitative differences between Fe/GaAs (or, in general, ferromagnet/zinc-blende semiconductor) based MTJs and other structures in which the Dresselhaus SOC is absent [e.g., Fe(001)/vacuum/bcc-Cu(001) in Ref. 27]. In fact, the interference of the Bychkov-Rashba and Dresselhaus interactions leads to a net anisotropic SOC with a C_{2v} symmetry which reflects the symmetry of the Fa/GaAs interface.[6,13] This observation is crucial because, as shown below, the C_{2v} symmetry of the SOCF (which is the underlying structure symmetry) is transferred into the tunneling magnetoresistance and results in a twofold symmetric in-plane TAMR. Based on these symmetry considerations we can conclude that the in-plane TAMR will exhibit a twofold symmetry in ferromagnet/semiconductor (F/S) based MTJs, while a fourfold symmetry in ferromagnet/insulator (F/I) based tunnel junctions [e.g., Fe/MgO/Fe, Fe(001)/vacuum/bcc-Cu(001), etc.] is expected (as long as the ferromagnet has cubic symmetry and additional uniaxial strain effects are negligible).

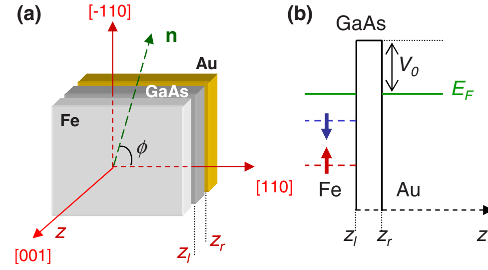

FIG. 3. (Color online) (a) Schematics of a Fe/GaAs/Au MTJ. The magnetization direction in the ferromagnet is specified by the vector **n**. (b) Schematics of the potential profile of the heterojunction along the [001] direction.

Motivated by the recent measurements of the in-plane TAMR in Fe/GaAs/Au MTJs (Fig. 3), we shall focus our discussion on the case of the in-plane TAMR in ferromagnet/semiconductor/normal-metal (F/S/NM) and in ferromagnet/semiconductor/ferromagnet ($F/S/F$) MTJs. Here and in what follows, when referring to a semiconductor (ferromagnet), a zinc-blende semiconductor (cubic metallic ferromagnet) is meant. Until now, all the theoretical investigations of the TAMR [with the exception of Refs. 6 and 13] have been based on first-principles calculations. We believe that, as a complement and inspiration to the first-principles approach, model calculations can be of great interest for a better understanding of the phenomenology of the TAMR effect. Because of the highly complicated band structure of F/S based heterojunctions, model calculations in such systems may appear as an oversimplified picture. However the relative simplicity and regularity of the angular dependence of the in-plane TAMR experimentally observed in Fe/GaAs/Au MTJs indicates that the TAMR may not depend strongly on the specific details of the complicated band structure, suggesting that some of the observed features of the TAMR effect could be understood on the basis of a simple minimal model. Thus, the model here proposed is not intended to completely describe all the details of the TAMR effect but to offer the simplest view which, by incorporating the spin-orbit interaction as the relevant physical mechanism, is capable of reproducing the main traits observed in the in-plane TAMR.

As mentioned above, in our model the twofold symmetry of the in-plane TAMR in F/S based MTJs originates from the interference of Dresselhaus and Bychkov-Rashba-type SOCs.[6,13] Such interference effects have already been investigated in lateral transport in two-dimensional (2D) electron systems,[30–32] in spin relaxation in quantum wells[33] and quantum dots,[34] or in 2D plasmons.[35] The symmetry, which is imprinted in the tunneling probability becomes apparent when a magnetic moment is present. Our main results are as follows: (i) finding analytical expressions for evaluating the in-plane TAMR in both $F/S/$NM and $F/S/F$ MTJs, (ii) prediction and evaluation of the in-plane ATMR in $F/S/F$ heterojunctions, and (iii) derivation of a simple phenomenological relation describing the dependence of the tunneling magnetoresistance on the absolute orientation of the in-plane magnetization(s) of the ferromagnet(s).

Since we are especially interested in the study of the in-plane TAMR and in-plane ATMR, and for the sake of brevity, in what follows we will refer to them as the TAMR and ATMR effects.

The paper is organized as follows. In Sec. II we present the theoretical model describing the tunneling through a MTJ. In a first approximation we consider the case of an infinitesimally thin barrier (Sec. II A), while the finite spatial extension of the potential barrier is incorporated in a more sophisticated approach discussed in Sec. II B. Detailed solutions and tunneling properties within these approximations are given in Appendixes A and B, respectively. In Sec. III we discuss the TAMR in both $F/S/$NM (Sec. III A) and $F/S/F$ (Sec. III B) MTJs. The ATMR in $F/S/F$ tunnel junctions is investigated in Sec. IV, where specific calculations for model Fe/GaAs/Fe MTJs are presented. In Sec. V we develop a phenomenological model for determining the dependence of the TAMR and ATMR on the absolute orientation(s) of the magnetization(s) in the ferromagnetic lead(s). Finally, conclusions are given in Sec. VI.

II. THEORETICAL MODEL

Consider an $F/S/F$ tunnel heterojunction in which the semiconductor lacks bulk inversion symmetry; zinc-blende semiconductors are typical examples. The bulk inversion asymmetry of the semiconductor together with the structure inversion asymmetry (for the case of asymmetric junctions) of the heterojunction give rise to the Dresselhaus[6,36–38] and Bychkov-Rashba[6,38,39] SOCs, respectively. The interference of these two spin-orbit interactions leads to a net anisotropic SOC with a C_{2v} symmetry which is imprinted onto the tunneling magnetoresistance as the electrons pass through the semiconductor barrier. This was discussed in some details in Refs. 6 and 13 for the case of $F/S/$NM tunnel junctions. Here we generalize the model proposed in Refs. 6 and 13 to the case of $F/S/F$ tunnel junctions. For such structures our model predicts the coexistence of both the TAMR and ATMR phenomena.

We consider an $F/S/F$ tunnel junction grown in the $z=[001]$ direction, where the zinc-blende semiconductor forms a barrier of width d between the left and right ferromagnetic electrodes. At first we discuss a simplified model for very thin barriers. In that case the barrier can be approximated by a Dirac-delta function and the SOC reduced to the plane of the barrier. In what follows we will refer to this model as the Dirac-delta function model (DDFM). A second model in which Slonczewski's proposal[3,6] for ferromagnet/insulator/ferromagnet tunnel junctions is generalized to the case of ferromagnet/semiconductor/ferromagnet junctions by including the Bychkov-Rashba and Dresselhaus SOCs will be referred to as the Slonczewski spin-orbit model (SSOM). In both the DDFM and the SSOM we assume coherent tunneling and a lattice mismatch small enough for the strain effects to be negligible. The fourfold anisotropy of the cubic metallic ferromagnet(s) is assumed to be much smaller than the tunneling anisotropic effects (this is particularly true in Fe/GaAs-based MTJs, where TAMR measurements have shown no trace of any fourfold anisotropy).[13]

A. DDFM

We consider here the case of a very thin tunneling barrier. Assuming that the in-plane wave vector $\mathbf{k}_{\parallel}$ is conserved throughout the heterostructure, one can decouple the motion along the growth direction (z) from the other spatial degrees of freedom. The effective model Hamiltonian describing the tunneling across the heterojunction reads as

$$H = H_0 + H_Z + H_{\mathrm{SO}}. \tag{7}$$

Here

$$H_0 = -\frac{\hbar^2}{2m_0}\frac{d^2}{dz^2} + V_0 d\,\delta(z), \tag{8}$$

with m_0 as the bare electron mass and V_0 and d as the height and width, respectively, of the actual potential barrier [here modeled with a Dirac-delta function $\delta(z)$] along the growth direction ($z=[001]$) of the heterostructure.

The spin splitting due to the exchange field in the left ($z<0$) and right ($z>0$) ferromagnetic regions is given by

$$H_Z = -\frac{\Theta(-z)\Delta_l}{2}\mathbf{n}_l\cdot\boldsymbol{\sigma} - \frac{\Theta(z)\Delta_r}{2}\mathbf{n}_r\cdot\boldsymbol{\sigma}. \tag{9}$$

Here Δ_l and Δ_r represent the exchange energy in the left and right ferromagnets, respectively, and $\Theta(z)$ is the Heaviside step function. The components of the vector $\boldsymbol{\sigma}$ are the Pauli matrices, and $\mathbf{n}_j=(\cos\theta_j,\sin\theta_j,0)$, with $j=l,r$, is a unit vector defining the in-plane magnetization direction in the left ($j=l$) and right ($j=r$) ferromagnets with respect to the [100] crystallographic direction. The Zeeman splitting in the semiconductor can be neglected.

In recent experiments with Fe/GaAs/Au tunnel junctions,[13] the reference axis was taken as the [110] direction. Therefore, it is convenient to express the magnetization direction relative to the [110] axis by introducing the angle shifting $\phi_j=\theta_j-\pi/4$ $(j=l,r)$. One can then write $\mathbf{n}_j=[\cos(\phi_j+\pi/4),\sin(\phi_j+\pi/4),0]$ with ϕ_j giving the magnetization direction in the left ($j=l$) and right ($j=r$) ferromagnets with respect to the [110] crystallographic direction.

Within the DDFM, the spin-orbit interaction throughout the semiconductor barrier (including the interfaces) can be written as

$$H_{SO} = (\mathbf{w}\cdot\boldsymbol{\sigma})\delta(z), \tag{10}$$

with the effective SOCF

$$\mathbf{w} = (-\bar{\alpha}k_y + \bar{\gamma}k_x,\ \ \bar{\alpha}k_x - \bar{\gamma}k_y,\ \ 0). \tag{11}$$

Here $\bar{\alpha}$ and $\bar{\gamma}$ represent effective values of the Bychkov-Rashba and linearized Dresselhaus parameters, respectively, and k_x and k_y refer to the x and y components of the wave vector $\mathbf{k}$. In terms of the usual Dresselhaus parameter γ, the linearized Dresselhaus parameter can be approximated[6] as $\bar{\gamma}\approx\gamma Q$, where $Q=2m_0V_0d/\hbar^2$ stands for the strength of the effective wave vector in the barrier.

In a real situation the barrier width is finite and there actually are two contributions of the interface Bychkov-Rashba SOC. Therefore there are two interface Bychkov-Rashba parameters α_l and α_r corresponding to the left and right interfaces, respectively. In the DDFM the two interfaces merge to form the Dirac-delta barrier with an effective Bychkov-Rashba parameter $\bar{\alpha}\approx\langle\alpha_l\delta(z)-\alpha_r\delta(z-d)\rangle_0$. Here the Dirac-delta functions account for the interface Bychkov-Rashba SOC in the real finite barrier with left and right interfaces at $z=0$ and $z=d$, respectively. The average $\langle\ldots\rangle_0$ refers to space and momentum averages with respect to the unperturbed states (i.e., in the absence of SOC) at the Fermi energy. Since the parameters α_l and α_r are not known for F/S and semiconductor/normal-metal (S/NM) interfaces, we still have to consider $\bar{\alpha}$ as a phenomenological parameter.

The scattering states in the left ($z<0$) and right ($z>0$) ferromagnetic regions are given by

$$\Psi_\sigma^{(l)} = \frac{e^{ik_\sigma z}\chi_\sigma^{(l)}}{\sqrt{k_\sigma}} + r_{\sigma,\sigma}e^{-ik_\sigma z}\chi_\sigma^{(l)} + r_{\sigma,-\sigma}e^{-ik_{-\sigma}z}\chi_{-\sigma}^{(l)}, \tag{12}$$

and

$$\Psi_\sigma^{(r)} = t_{\sigma,\sigma}e^{i\kappa_\sigma z}\chi_\sigma^{(r)} + t_{\sigma,-\sigma}e^{i\kappa_{-\sigma}z}\chi_{-\sigma}^{(r)}, \tag{13}$$

respectively. Here we have introduced the wave-vector components

$$k_\sigma = \sqrt{\frac{2m_0}{\hbar^2}\left(E+\sigma\frac{\Delta_l}{2}\right) - k_\parallel^2}, \tag{14}$$

and

$$\kappa_\sigma = \sqrt{\frac{2m_0}{\hbar^2}\left(E+\sigma\frac{\Delta_r}{2}\right) - k_\parallel^2}, \tag{15}$$

with $k_\parallel=\sqrt{k_x^2+k_y^2}$ denoting the length of the wave-vector component corresponding to the free motion in the x-y plane. The spinors

$$\chi_\sigma^{(j)} = \frac{1}{\sqrt{2}}\begin{pmatrix}1\\ \sigma e^{i(\phi_j+\pi/4)}\end{pmatrix}\quad (j=l,r), \tag{16}$$

correspond to a spin parallel ($\sigma=\uparrow$) or antiparallel ($\sigma=\downarrow$) to the magnetization direction $\mathbf{n}_j=[\cos(\phi_j+\pi/4),\sin(\phi_j+\pi/4),0]$ in the left ($j=l$) and right ($j=r$) ferromagnets.

Here and in what follows, we consider a free-electron behavior for the in-plane wave vector $k_\parallel$, which is a simplified view of the actual band structure. Such an approximation may not be appropriate for describing systems or phenomena in which the contribution of states with large $k_\parallel$ is relevant. For the system considered here we expect that the main contribution to TAMR comes from the states with small $k_\parallel$. This expectation is based on the fact that the experimentally observed magnetization-direction dependence of the TAMR in Fe/GaAs based MTJs exhibits a twofold symmetry with only two *lobes* [see Figs. 2(a) and 2(b) of Ref. 13], indicating that only the lowest nonvanishing order in the SOCF is relevant. If, for example, higher orders in the SOCF terms (which are also higher in k_x and k_y) were relevant for the transmissivity, the corresponding symmetry of the SOCF would lead to a twofold symmetric TAMR but with four lobes instead of the only two that are observed experimentally. The absence of traces of higher order in the SOCF terms in the observed TAMR suggests that the states with large $k_\parallel$ do not play a significant role.

The reflection and transmission coefficients can be found by imposing appropriate boundary conditions and solving the corresponding system of linear equations (for details see Appendix A). The transmissivity of an incoming spin-σ particle can then be evaluated from the relation

$$T_\sigma(E,k_\parallel) = \mathrm{Re}[\kappa_\sigma(|t_{\sigma,\sigma}|^2 + \kappa_{-\sigma}|t_{\sigma,-\sigma}|^2)]. \tag{17}$$

Explicit analytical expressions for the transmission coefficients ($t_{\sigma,\sigma}$ and $t_{\sigma,-\sigma}$) are given in Appendix A.

B. SSOM

We present a generalization of the Slonczewski model[3] for ferromagnet/insulator/ferromagnet tunnel junctions to the case in which the insulator barrier is replaced by a zinc-blende semiconductor. Unlike in the DDFM, now the spatial extension of the potential barrier is taken into account. The model Hamiltonian is

$$H = H_0 + H_Z + H_{BR} + H_D, \tag{18}$$

where

$$H_0 = -\frac{\hbar^2}{2}\nabla\left[\frac{1}{m(z)}\nabla\right] + V_0\Theta(z)\Theta(d-z). \tag{19}$$

The electron effective mass $m(z)$ is assumed to be $m=m_c$ in the central (semiconductor) region and $m=m_0$ in the ferromagnets. The exchange splitting in the ferromagnets is now given by

$$H_Z = -\frac{\Theta(-z)\Delta_l}{2}\mathbf{n}_l\cdot\boldsymbol{\sigma} - \frac{\Theta(z-d)\Delta_r}{2}\mathbf{n}_r\cdot\boldsymbol{\sigma}. \tag{20}$$

The Dresselhaus SOC can be written as[6,37,38,40,41]

$$H_D = (k_x\sigma_x - k_y\sigma_y)\frac{\partial}{\partial z}\left(\gamma(z)\frac{\partial}{\partial z}\right), \tag{21}$$

where x and y correspond to the [100] and [010] directions, respectively. The Dresselhaus parameter $\gamma(z)$ has a finite value γ in the semiconductor region, where the bulk inversion asymmetry is present and vanishes elsewhere. Note that because of the steplike spatial dependence of $\gamma(z)$, the Dresselhaus SOC [Eq. (21)] implicitly includes both the interface and bulk contributions.[6,37,41]

The Bychkov-Rashba SOC is given by[42]

$$H_{\rm BR} = [\alpha_l \delta(z - z_l) - \alpha_r \delta(z - z_r)](k_x \sigma_y - k_y \sigma_x), \quad (22)$$

and arises due to the F/S interface inversion asymmetry.[6] Here α_l (α_r) denotes the SOC strength at the left (right) interface $z_l=0$ ($z_r=d$). For the small voltages considered here (up to a hundred mV), the Bychkov-Rashba SOC inside the semiconductor can be neglected.

The z components of the scattering states in the left and right ferromagnets have the same form as in Eqs. (12) and (13), respectively.

In the central (semiconductor) region ($0<z<d$) we have

$$\Psi_\sigma^{(c)} = \sum_{i=\pm} (A_{\sigma,i} e^{q_i z} + B_{\sigma,i} e^{-q_i z}) \chi_i^{(c)}, \quad (23)$$

$$\chi_\pm^{(c)} = \frac{1}{\sqrt{2}} \begin{pmatrix} 1 \\ \pm e^{i\xi} \end{pmatrix}. \quad (24)$$

The angle ξ is defined through the relation $\tan(\xi)=-k_y/k_x$. We have also used the notation

$$q_\pm = \frac{q_0}{\sqrt{1 \mp \left(\frac{2m_c \gamma k_\parallel}{\hbar^2}\right)^2}}, \quad (25)$$

where

$$q_0 = \sqrt{\frac{2m_c(V_0 - E)}{\hbar^2} + k_\parallel^2} \quad (26)$$

is the length of the z component of the wave vector in the barrier in the absence of SOC.

The expansion coefficients in Eqs. (12), (13), and (23) can be found by applying appropriate matching conditions at each interface and by solving the corresponding system of linear equations [for details, see Eq. (A35)]. Once the wave function is determined, the particle transmissivity can be calculated from Eq. (17). Approximate analytical expressions for the transmission coefficients $t_{\sigma,\sigma}$ and $t_{\sigma,-\sigma}$ are given in Appendix B.

III. TAMR

The magnetoresistance of a tunnel junction can be obtained by evaluating the current through the device or the conductance. The current flowing along the heterojunction is given by

$$I = \frac{e}{(2\pi)^3 \hbar} \sum_{\sigma=\uparrow,\downarrow} \int dE d^2\mathbf{k}_\parallel T_\sigma(E,\mathbf{k}_\parallel)[f_l(E) - f_r(E)], \quad (27)$$

where $f_l(E)$ and $f_r(E)$ are the Fermi-Dirac distributions with chemical potentials μ_l and μ_r in the left and right (metallic or ferromagnetic) leads, respectively. For the case of zero temperature and small voltages, the Fermi-Dirac distributions can be expanded in powers of the voltage $V_{\rm bias}$. To first order in $V_{\rm bias}$ one obtains $f_l(E)-f_r(E) \approx \delta(E-E_F)V_{\rm bias}$, with $\delta(x)$ as the Dirac-delta function and E_F as the Fermi energy. One then obtains the following approximate expression for the conductance:

$$G = \sum_{\sigma=\uparrow,\downarrow} G_\sigma, \quad G_\sigma = \frac{e^2}{(2\pi)^3 \hbar} \int d^2\mathbf{k}_\parallel T_\sigma(E_F,\mathbf{k}_\parallel). \quad (28)$$

We note that although similar, the expression above differs from the linear-response conductance.

In our model, the transmissivity $T_\sigma(E_F,\mathbf{k}_\parallel)$ depends on the voltage via the voltage dependence of the Bychkov-Rashba parameter $\bar{\alpha}$.[43] Recent first-principles calculations[44] have shown that the SOCF is different for different bands; therefore the effective value of $\bar{\alpha}$ is energy dependent. By applying an external voltage the energy window relevant for tunneling can be changed, resulting in voltage-dependent values of $\bar{\alpha}$ and, therefore, in a voltage dependence of the transmissivity. Consequently, the conductance in Eq. (28) depends, parametrically, on the applied voltage.

A. TAMR in ferromagnet/semiconductor/normal-metal tunnel junctions

The tunneling properties of $F/S/$NM junctions can be obtained as a limit case of the models proposed in Sec. II for $F/S/F$ tunnel junctions by taking $\phi_l=\phi_r=\phi$ and Δ_r as the Zeeman splitting in the normal-metal region. In the present case l, c, and r refer to the ferromagnetic (left), semiconductor (central), and normal-metal (right) regions, respectively.

The TAMR in $F/S/$NM tunnel junctions refers to the changes in the tunneling magnetoresistance (R) when varying the magnetization direction $\mathbf{n}_l$ of the magnetic layer with respect to a fixed axis. Here we assume the [110] crystallographic direction as the reference axis. The TAMR is then given by[6]

$$\text{TAMR}_{[110]}(\phi) = \frac{R(\phi) - R(0)}{R(0)} = \frac{G(0) - G(\phi)}{G(\phi)}. \quad (29)$$

Since in a $F/S/$NM tunnel junction only one electrode is magnetic, the conventional TMR effect is absent.

An alternative to the magnetoresistance, which refers to the charge transport, is the spin-polarization efficiency of the transmission characterized by the tunneling spin polarization,[4,5]

$$P = \frac{I_\uparrow - I_\downarrow}{I}, \quad (30)$$

where I_σ is the charge current corresponding to the spin-σ channel and I is the total current. The changes in the tunneling spin polarization when the magnetization of the ferromagnet is rotated in plane can then be characterized by the tunneling anisotropic spin polarization (TASP), which is defined as[6]

$$\text{TASP}_{[110]}(\phi) = \frac{P(0) - P(\phi)}{P(\phi)}. \quad (31)$$

Taking into account that the Zeeman splitting in the normal metal is small we can approximate $\kappa_\sigma \approx \kappa_{-\sigma}$ and the total conductance can be written as the sum of isotropic ($G^{\rm iso}$) and anisotropic [$G^{\rm aniso}(\phi)$] contributions (for details see Appendix A). It follows then from Eq. (29) that the TAMR is given by

$$\mathrm{TAMR}_{[110]}(\phi) = \frac{G^{\mathrm{aniso}}(0) - G^{\mathrm{aniso}}(\phi)}{G^{\mathrm{iso}} + G^{\mathrm{aniso}}(\phi)}. \quad (32)$$

For junctions in which the Bychkov-Rashba and Dresselhaus SOCs can be considered as small perturbations, the anisotropy is small and $G^{\mathrm{aniso}}(\phi) \ll G^{\mathrm{iso}}$. In addition, the SOC effects on the isotropic part of the conductance is also small and $G^{\mathrm{iso}} \approx G^{(0)}$ (here $G^{(0)}$ denotes the conductance in the absence of the SOC). The TAMR can then be approximated as

$$\mathrm{TAMR}_{[110]}(\phi) \approx \frac{G^{\mathrm{aniso}}(0) - G^{\mathrm{aniso}}(\phi)}{G^{(0)}}. \quad (33)$$

The substitution of Eq. (A17) into Eq. (33) leads to

$$\mathrm{TAMR}_{[110]}(\phi) \approx \frac{e^2}{h} \frac{\langle g_{2\uparrow} k_\parallel^2 \rangle_\uparrow + \langle g_{2\downarrow} k_\parallel^2 \rangle_\downarrow}{G^{(0)}} \lambda_\alpha \lambda_\gamma [\cos(2\phi) - 1]. \quad (34)$$

Here we have introduced the dimensionless SOC parameters $\lambda_\alpha = 2m_0\bar{\alpha}/\hbar^2$ and $\lambda_\gamma = 2m_0\bar{\gamma}/\hbar^2$. The functions $g_{2\uparrow}$ and $g_{2\downarrow}$ are given by Eq. (A18).

The expression above gives the angular dependence of the TAMR and is consistent with the angular dependence experimentally observed in Fa/GaAs/Au tunnel junctions.[13] It also suggests that the inversion (change in sign) of the TAMR (such an inversion has been experimentally observed[13]) may originate from bias-induced changes in the product $\lambda_\alpha \lambda_\gamma \propto \bar{\alpha}\bar{\gamma}$. In general, the bias dependence of the Dresselhaus parameter in semiconductors is weak, while the Bychkov-Rashba parameter can be tuned by varying the voltage. Thus, we consider in our model that the possible change in sign of the $\mathrm{TAMR}_{[110]} \propto \lambda_\alpha \lambda_\gamma$ is determined by bias-induced changes in the sign of the effective Bychkov-Rashba parameter $\bar{\alpha}$. Furthermore, one can see from Eq. (34) that the amplitude of the TAMR is governed by the product $\lambda_\alpha \lambda_\gamma \propto \bar{\alpha}\bar{\gamma}$ and the averages $\langle g_{2\sigma} k_\parallel^2 \rangle_\sigma$ $(\sigma = \uparrow, \downarrow)$. When $\bar{\alpha}\bar{\gamma} = 0$, the twofold TAMR is suppressed (the suppression of the TAMR was also observed in Ref. 13), i.e., as long as other anisotropic effects such as uniaxial strain are not present, the Bychkov-Rashba (or Dresselhaus) SOC alone cannot explain the experimentally observed C_{2v} symmetry of the TAMR. The TAMR vanishes also if the spin polarization of both electrodes becomes sufficiently small. In such a case $k_{F,\uparrow} \approx k_{F,\downarrow}$ and $g_{2\sigma}$ vanishes [see Eq. (A18)], resulting in the suppression of the TAMR. On the contrary, Eq. (34) predicts an increase in the TAMR amplitude for $F/S/\mathrm{NM}$ tunnel junctions whose constituents exhibit large values of $\bar{\alpha}\bar{\gamma}$ as well as a large spin polarization in the magnetic electrode.

A simple intuitive explanation of the origin of the uniaxial anisotropy of the TAMR can be obtained by investigating the dependence of the effective SOCF $\mathbf{w}(\mathbf{k}_\parallel)$ [see Eq. (11)], i.e., the effective magnetic field that the spins feel when traversing the semiconducting barrier. A schematics of the anisotropy of the SOCF $\mathbf{w}(\mathbf{k}_\parallel)$ is shown in Fig. 4(a), where the thin arrows represent a vector plot of $\mathbf{w}(\mathbf{k}_\parallel)$, while the solid line is a polar plot of the field amplitude $|\mathbf{w}(\mathbf{k}_\parallel)|$ for a fixed value of $k_\parallel = |\mathbf{k}_\parallel|$. The SOCF is oriented in the [110] ([−110]) direction at the points of low (high) SOCF, where the field amplitude $|\mathbf{w}|$ reaches a minimum (maximum).

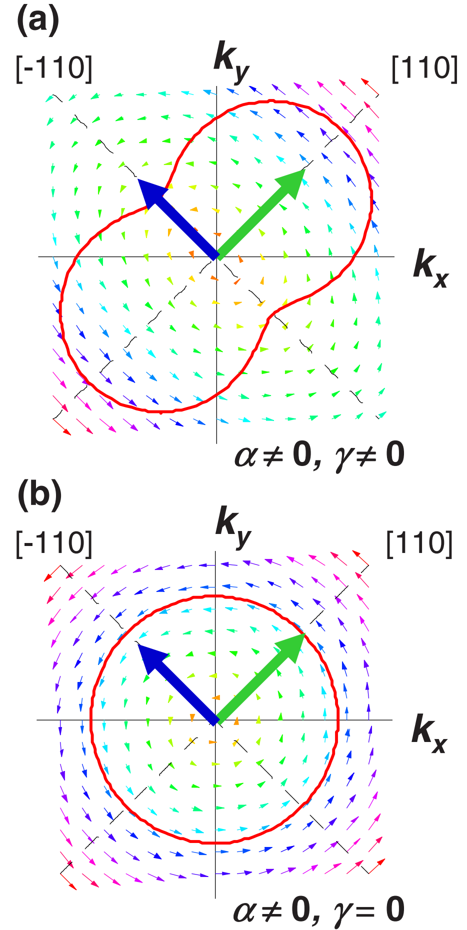

FIG. 4. (Color online) (a) Schematics of the anisotropy of the spin-orbit coupling field $\mathbf{w}(\mathbf{k}_\parallel)$ when both the Bychkov-Rashba and Dresselhaus SOCs are present $(\alpha, \gamma \neq 0)$. Thin arrows represent a vector plot of the SOCF $\mathbf{w}$. The solid line is a polar plot of the SOCF strength $|\mathbf{w}(\mathbf{k}_\parallel)|$ for a fixed value of $k_\parallel = |\mathbf{k}_\parallel|$. When the magnetization of the ferromagnet points along the [−110] direction [see thick blue (black) arrow], the direction of the strongest SOCF is parallel to the incident majority spins which easily tunnel through the barrier. On the contrary, for a magnetization direction [110] [see thick green (gray) arrow], the strongest SOCF is perpendicular to the incident spins and the tunneling becomes less favorable. The net result is a spin-valve effect whose efficiency depends upon the absolute orientation of the magnetization and gives rise to the in-plane TAMR. (b) Same as in (a) but in the absence of Dresselhaus SOC $(\alpha \neq 0,\ \gamma = 0)$. In this case the amplitude of the SOCF $|\mathbf{w}(\mathbf{k}_\parallel)|$ becomes isotropic and the in-plane TAMR is suppressed.

When the magnetization in the ferromagnet points along the [−110] direction, the direction of the highest SOCF is parallel to the incident, majority spins which are then easily transmitted through the barrier. On the other hand, for a magnetization direction [110], the highest SOCF is perpendicular to the incident spins (to both the majority and minority spins) and the transmission becomes less favorable than in the case the magnetization is in the [−110] direction. This spin-orbit-induced difference in the tunneling transmissivities depending on the magnetization direction results in the uniaxial anisotropy of the TAMR.[45] We remark that this effect relies on the uniaxial anisotropy of the SOCF amplitude $|\mathbf{w}|$, which is

a consequence of the interference of the Bychkov-Rashba and Dresselhaus SOC. In systems such as Fe(001)/vacuum/bcc-Cu(001), in which the Dresselhaus SOC is absent, the linear in k_x and k_y Bychkov-Rashba terms lead to an isotropic SOCF amplitude [see Fig. 4(b)] and the effect is absent. Thus for such systems no in-plane TAMR is expected to occur unless higher-order SOC terms become relevant. However, even in such a case the TAMR will exhibit a fourfold symmetry compatible with the C_{4v} symmetry of the general Bychkov-Rashba SOCF.

The magnetization-direction dependence of the transmission and reflection of the incident spins should be reflected in the local density of states at the interfaces of the barrier. Within the DDFM the left (F/S) and right (S/NM) interfaces are merged into a single plane and one cannot distinguish between them. A more detailed view of the role of the interfaces requires the use of the SSOM. It turns out (this will be shown later in this section) that the F/S interface plays a major role in the TAMR phenomenon while the S/NM interface appears irrelevant. This is intuitively expected since the exchange splitting in the ferromagnet is much larger than the Zeeman splitting in the normal metal. Consequently, the spin-valve effect at the F/S interface is much stronger than in the S/NM interface.

The local density of states reflects also the uniaxial anisotropy of the TAMR with respect to the magnetization orientation in the ferromagnet. In fact, one can introduce the anisotropic local density of states (ALDOS) through the definition

$$\mathrm{ALDOS}_{[110]}(z,\phi) = \frac{\mathrm{LDOS}(z,0) - \mathrm{LDOS}(z,\phi)}{\mathrm{LDOS}(z,\phi)}, \quad (35)$$

where

$$\mathrm{LDOS}(z,\phi) = \sum_{\sigma=\uparrow,\downarrow} \int \frac{d\mathbf{k}_\parallel}{(2\pi)^2} |\Psi_\sigma(z,\phi,k_{\sigma F})|^2 \quad (36)$$

is the total local density of states at position z and evaluated at the Fermi surface determined by the Fermi wave vectors

$$k_{\sigma F} = \sqrt{\frac{2m_0}{\hbar^2}\left(E_F + \sigma\frac{\Delta_l}{2}\right) - k_\parallel^2}. \quad (37)$$

Since we are interested only in propagating states, we may restrict the possible values of $k_\parallel$ to the interval $[0, k_{\max}^\sigma]$, with $k_{\max}^\sigma$ given by Eq. (A16). Since the spin splitting in the normal-metal region is negligibly small, $\kappa_\sigma \approx \kappa_{-\sigma}$. It follows from Eqs. (13) and (17) that

$$T_\sigma(E,k_\parallel) \propto |\Psi_\sigma^{(r)}|^2, \quad (38)$$

and, therefore, the conductance [see Eq. (28)] is related to the LDOS at $z=d$ as $G_\sigma(\phi) \propto \mathrm{LDOS}(d,\phi)$. One then obtains that

$$\mathrm{TAMR}_{[110]}(\phi) \approx \mathrm{ALDOS}_{[110]}(z=d,\phi). \quad (39)$$

For a numerical illustration we consider an epitaxial Fe/GaAs/Au heterojunction similar to that used in the experimental observations reported in Ref. 13. We use the value $m_c=0.067\ m_0$ for the electron effective mass in the central

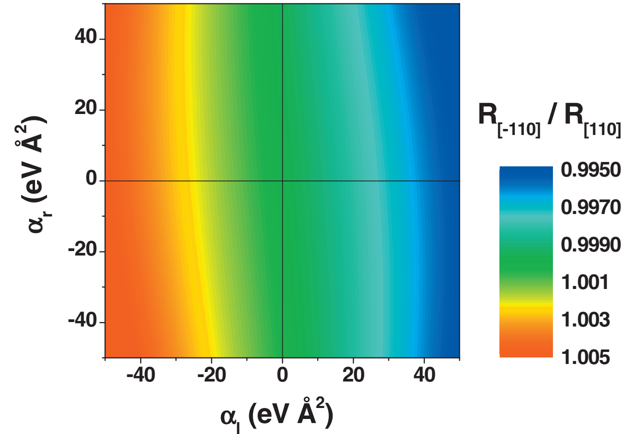

FIG. 5. (Color) Values of the ratio $R_{[\bar{1}10]}/R_{[110]}$ as a function of the interface Bychkov-Rashba parameters α_l and α_r.

(GaAs) region. The barrier width and height (measured from the Fermi energy) are, respectively, $d=80$ Å and $V_c=0.75$ eV, corresponding to the experimental samples in Ref. 13. For the Fe layer a Stoner model with the majority- and minority-spin channels having Fermi momenta $k_{F\uparrow}=1.05\times10^8\ \mathrm{cm}^{-1}$ and $k_{F\downarrow}=0.44\times10^8\ \mathrm{cm}^{-1}$,[46] respectively, is assumed. The Fermi momentum in Au is taken as $\kappa_F=1.2\times10^8\ \mathrm{cm}^{-1}$.[47] We consider the case of relatively weak magnetic fields (specifically, $B=0.5$ T). At high magnetic fields, say, several Tesla, our model is invalid as it does not include cyclotron effects which become relevant when the cyclotron radius approaches the barrier width.

The Dresselhaus spin-orbit parameter in GaAs is $\gamma \approx 24$ eV Å^3.[6,38,40] On the other hand, the values of the interface Bychkov-Rashba parameters α_l and α_r [see Eq. (22)] are not known for metal-semiconductor interfaces. Due to the complexity of the problem, a theoretical estimation of such parameters requires first-principles calculations including the band-structure details of the involved materials,[44] which are beyond the scope of the present paper. Here we assume α_l and α_r as phenomenological parameters which must be understood as the values of the interface Bychkov-Rashba parameters at the F/S and S/NM interfaces, respectively, averaged over all the relevant bands contributing to the transport across the corresponding interfaces. In order to investigate how does the degree of anisotropy depend on these two parameters we performed calculations of the ratio $R_{[\bar{1}10]}/R_{[110]}$ (which is a measure of the degree of anisotropy[13]) as a function of α_l and α_r by using the spin-orbit Slonczewski model described in Sec. II B. The results are shown in Fig. 5, where one can appreciate that the size of this ratio (and, consequently, of the TAMR) is dominated by α_l. This is because the Zeeman splitting in Au is very small compared to the exchange splitting in Fe and, consequently, the spin flips mainly when crossing the F/S interface. Then, since the values of the TAMR are not very sensitive to the changes in α_r we can set this parameter, without loss of generality, to zero. This leaves α_l as a single fitting parameter when comparing to experiment. The values of the phenomenological parameter α_l were determined in Refs. 6 and 13 by fitting the theory to the experimental value of the ratio $R_{[-110]}/R_{[110]}$,

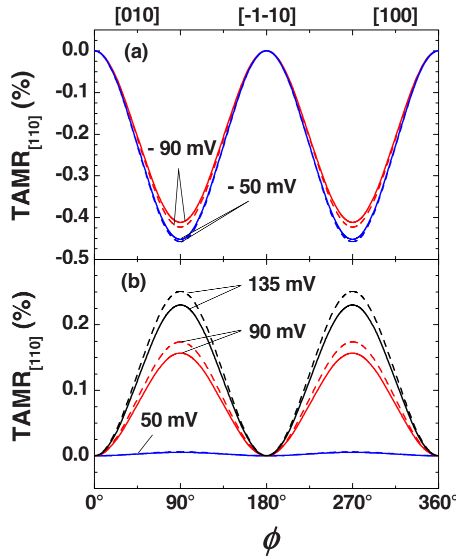

FIG. 6. (Color online) Model calculations of the angular dependence of the TAMR in a Fe/GaAs/Au MTJ. Solid and dashed curves represent the results obtained within the SSOM and the DDFM, respectively. (a) For α_l=42.3 eV Å^2 and α_l=45.8 eV Å^2 which correspond to voltages −90 and −50 mV, respectively (Ref. 13). (b) For α_l=−0.6 eV Å^2, α_l=−17.4 eV Å^2, and α_l=−25.1 eV Å^2 corresponding to voltages 50, 90, and 135 mV, respectively (Ref. 13).

and a very satisfactory agreement between theory and experiment was achieved. This fitting at a single angle was enough for the theoretical model to reproduce the *complete* angular dependence of the TAMR, demonstrating the robustness of the model.

Assuming that the interface Bychkov-Rashba parameter α_l is voltage dependent and performing the fitting procedure for different values of the bias voltage, the bias dependence of α_l can be extracted.[6,13] Here we use the same values of α_l reported in Refs. 6 and 13 for computing the angular dependence of the TAMR at different values of the bias voltage. The results are shown in Fig. 6, where the dashed and solid lines correspond to calculations within the DDFM and the SSOM, respectively. An overall agreement between the two models can be appreciated. The TAMR exhibits an oscillatory behavior as a function of the magnetization direction [see also Eq. (34)] and can be inverted by changing the bias voltage [compare Figs. 6(a) and 6(b)]. This bias-induced inversion of the TAMR was experimentally observed in Fe/GaAs/Au tunnel junctions[13] and was explained to occur as a consequence of a bias-induced change in the sign of the effective Bychkov-Rashba parameter. Preliminary *ab initio* calculations[44] for Fe/GaAs structures suggest that the Bychkov-Rashba parameters associated with different bands may have different values and even change the sign. Thus, the effective value of the interface Bychkov-Rashba parameter α_l will depend on which bands are the ones that mainly contribute to the transport across the Fe/GaAs interface (at low temperature those are the ones which have the appropriate symmetry and lie inside the voltage window around the Fermi energy). For different values of the bias voltage different set of bands will be relevant to transport. On the other hand, to different set of bands correspond, in our model,

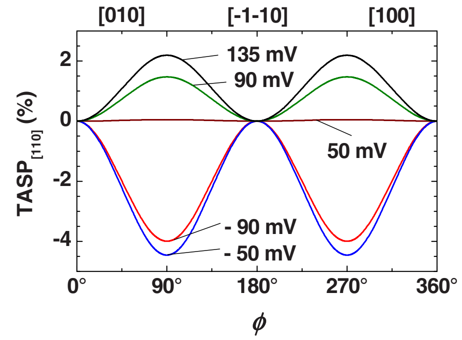

FIG. 7. (Color online) Model calculations of the angular dependence of the TASP in a Fe/GaAs/Au MTJ for different values of the bias voltage.

different effective values of the interface Bychkov-Rashba parameter and therefore different transmissivities [recall the transmissivity in Eq. (28) is a function of the interface Bychkov-Rashba parameter]. Consequently, both α_l and the transmissivity becomes strongly dependent on the bias voltage. The above analysis suggests that the inversion of the TAMR may originate from the bias-induced sign change of the effective Bychkov-Rashba SOC at the Fe/GaAs interface (or, rather, its product with the Dresselhaus SOC), as proposed in Refs. 6 and 13. However, more investigations are still needed to fully understand the inversion of the TAMR in Fe/GaAs based MTJs.

The sign change of the effective Bychkov-Rashba parameter has also influence on the tunneling spin polarization, resulting in the bias-induced inversion (change in sign) of the TASP as shown in Fig. 7. Bias-induced changes in the sign of the tunneling spin polarization in Fe(001)/vacuum/bcc-Cu(001) MTJs have also been reported.[27] The anisotropy of the tunneling spin polarization, which also exhibits a twofold symmetry, indicates that the amount of transmitted and reflected spin at the interfaces depends on the magnetization direction in the Fe layer, resulting in an anisotropic local density of states at the Fermi surface. This is consistent with previous works[9,10,15] in which the anisotropy of the density of states with respect to the magnetization direction was related to the origin of the TAMR. In fact, our model calculations reveal that the TAMR, ALDOS [see Eq. (39)], and TASP all exhibit a C_{2v} symmetry with the same kind of angular dependence (compare Figs. 6 and 7).

A system parameter that can influence the size of the TAMR is the width of the barrier. The angular dependence of the TAMR calculated within the SSOM for the case of V_{bias}=−90 meV is displayed in Fig. 8(a) for different values of the barrier width d. As one would expect, the changes in the barrier width do not affect the twofold symmetry of the TAMR but only its amplitude, whose absolute value is predicted to increase when increasing the width of the barrier [see Fig. 8(b)].

We remark that our model neglects the contribution of the spin-orbit-induced symmetries of the involved bulk structures. Say, Fe exhibits a fourfold anisotropy, which should be reflected in the tunneling density of states. The fact that this is not seen in the experiment suggests that this effect is smaller than the twofold symmetry considered in our model.

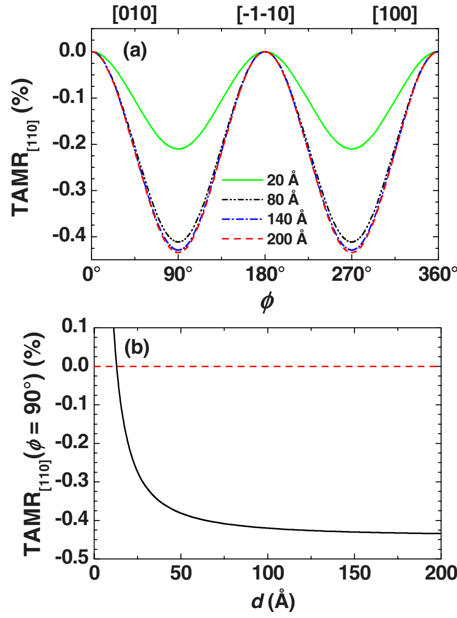

FIG. 8. (Color online) (a) Model calculations of the angular dependence of the TAMR in a Fe/GaAs/Au MTJ for different values of the barrier width d and a bias voltage $V_{\mathrm{bias}}=-90$ mV ($\alpha_l=42.3$ eV Å^2). (b) Amplitude of the TAMR (at $\phi=90°$) as a function of the barrier width. The TAMR curves were obtained by using the SSOM.

B. TAMR in ferromagnet/semiconductor/ferromagnet tunnel junctions

Our discussion in Sec. III A suggests that in the case of a $F/S/F$ tunnel junction, the magnetoresistance will depend on the absolute direction of the magnetization in each of the ferromagnets. In the left and right electrodes, the magnetization directions with respect to the [110] crystallographic direction are given by the angles $\phi=\phi_l$ and ϕ_r, respectively. For convenience we introduce the angle $\theta=\phi_r-\phi_l$, describing the magnetization direction in the right ferromagnet relative to that in the left ferromagnet (see Fig. 9). Different values of the tunneling magnetoresistance are expected to occur when in-plane rotating the magnetizations of both ferromagnets at the same time while keeping the relative angle θ fixed. Thus, the expression for the TAMR in $F/S/\mathrm{NM}$ junctions [see Eq. (29)] can now be generalized as

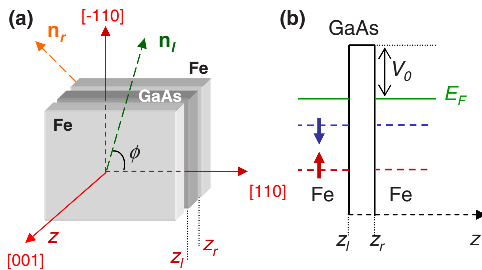

FIG. 9. (Color online) (a) Schematics of a Fe/GaAs/Fe MTJ. The magnetization direction in the left (right) ferromagnet is specified by the vector $\mathbf{n}_l$ ($\mathbf{n}_r$). (b) Schematics of the potential profile of the heterojunction along the [001] direction.

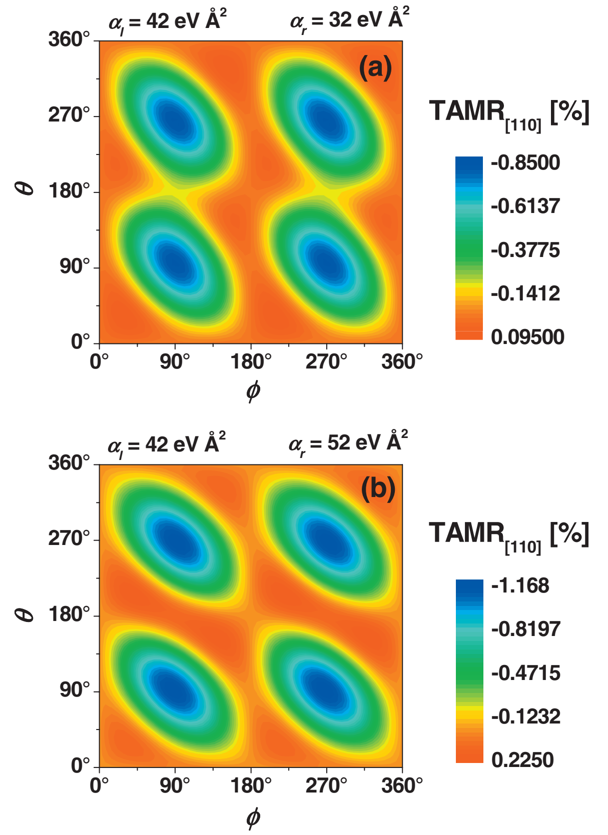

FIG. 10. (Color) Model calculations of the TAMR defined in Eq. (40) in a Fe/GaAs/Fe MTJ as a function of the angles ϕ and θ. (a) For $\alpha_l=42$ eV Å^2 and $\alpha_r=32$ eV Å^2 (i.e., $\bar{\alpha}>0$). (b) For $\alpha_l=42$ eV Å^2 and $\alpha_r=52$ eV Å^2 (i.e., $\bar{\alpha}<0$).

$$\mathrm{TAMR}_{[110]}(\theta,\phi)=\frac{R(\theta,\phi)-R(\theta,0)}{R(\theta,0)}=\frac{G(\theta,0)-G(\theta,\phi)}{G(\theta,\phi)}. \tag{40}$$

Following the same procedure as in Sec. III A, one can, in principle, obtain analytical expressions for the TAMR in a $F/S/F$ junction. It turns out however that in the general case defined by Eq. (40) the resulting relations are quite lengthy and not much simpler than the more accurate expressions obtained within the SSOM (see Appendix B). Therefore, we omit here the expressions resulting from the DDFM and show only the results obtained within the SSOM.

The dependence of the TAMR on the angles θ and ϕ is shown in Fig. 10 for the case of a Fe/GaAs/Fe MTJ. The width of the barrier is $d=80$ Å. Two different cases, corresponding to (a) $\bar{\alpha}>0$ and (b) $\bar{\alpha}<0$, are considered. In both cases, the absolute value of the TAMR reaches its maximal amplitude when the magnetization of the left electrode is parallel to the $[-110]$ direction (i.e., $\phi=90°,270°$) and the one of the right electrode is perpendicular to it (i.e., $\theta=90°,270°$). This is because this configuration, in our parabolic model, corresponds to the case of the stronger structure inversion asymmetry and, consequently, to the largest absolute value of the effective Bychkov-Rashba parameter $\bar{\alpha}$. We also note that at a fixed value of θ the TAMR has a twofold

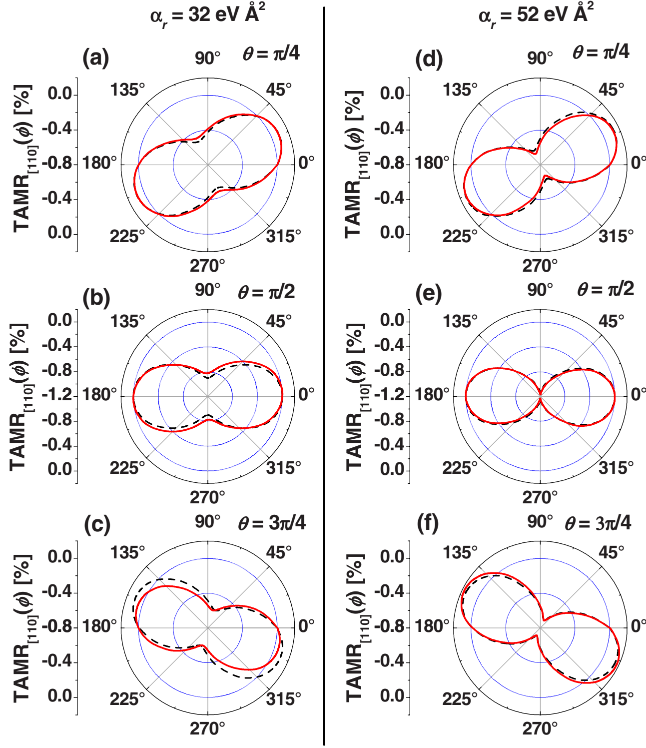

FIG. 11. (Color online) Model calculations of the angular dependence of the TAMR in a Fe/GaAs/Fe MTJ for fixed values of the angle θ between the electrode and counterelectrode magnetizations. The figures correspond to polar plots of the traces $\theta=\pi/4$, $\theta=\pi/2$, and $\theta=3\pi/4$ of Fig. 10. Solid lines correspond to the calculations within the SSOM, while dashed lines are obtained from the phenomenological model by using Eqs. (60)–(62).

symmetry with respect to ϕ and vice versa. It is clear, however, that the angles θ and ϕ play different roles in the symmetry of the TAMR, which manifest in the lack of mirror symmetry with respect to the axis $\theta=\phi$. We have investigated some traces of the TAMR displayed in Fig. 10. The results are shown in Fig. 11 where we present polar plots of the TAMR as a function of ϕ for fixed values of θ. The solid lines correspond to the calculations within the SSOM. The meaning of the dashed lines will be explained in Sec. V. The orientation of the symmetry axis of the twofold symmetric TAMR is determined by the relative angle θ rather than by the relative values of the interface Bychkov-Rashba parameters (note for the same θ, the symmetry axis does not change its orientation with α_r). The amplitude of the TAMR is bigger for the case of $\alpha_r=52$ eV Å^2 than for $\alpha_r=32$ eV Å^2 and shows a strong dependence on θ.

IV. ATMR

We now consider the SOC effects on the TMR for the case of a $F/S/F$ tunnel junction. The *conventional* TMR effect in ferromagnet/insulator/ferromagnet ($F/I/F$) tunnel junctions relies on the dependence of the magnetoresistance across the junction on the relative magnetization directions in the different ferromagnetic layers and their spin polarizations.[3,6]

In the case of $F/S/F$ heterojunctions, the interference between Bychkov-Rashba and Dresselhaus SOCs leads to anisotropic effects. Consequently, the conventional TMR in $F/S/F$ junctions will depend not only on the relative but also on the absolute magnetization directions in the ferromagnets, resulting in an anisotropic magnetoresistance. For quantifying this phenomenon we introduced the ATMR ratio defined in Eq. (4) which in terms of conductance reads as

$$\mathrm{ATMR}_{[110]} = \frac{G_{\mathrm{P}}(\phi) - G_{\mathrm{AP}}(\phi)}{G_{\mathrm{AP}}(\phi)} \tag{41}$$

and accounts for the magnetoresistance dependence on the absolute magnetization orientations with respect to the [110] crystallographic direction (see Fig. 9). Furthermore, the efficiency η of the anisotropic effects on the tunneling magnetoresistance can be defined as

$$\eta = \frac{\mathrm{ATMR}_{[110]}(\phi) - \mathrm{ATMR}_{[110]}(0)}{\mathrm{ATMR}_{[110]}(0)}. \tag{42}$$

A simplified approximate expression for the ATMR can be found within the DDFM by following the same procedure as in Sec. III A. The result is

$$\mathrm{ATMR}_{[110]} \approx \mathrm{TMR} - \frac{e^2}{hG_{\mathrm{AP}}^{(0)}}\left[\frac{(\lambda_\alpha^2+\lambda_\gamma^2)}{2}\sum_{\sigma=\uparrow,\downarrow}\langle(g_{1\sigma}^{\mathrm{P}}-g_{1\sigma}^{\mathrm{AP}})k_\parallel^2\rangle_\sigma + \lambda_\alpha\lambda_\gamma\cos(2\phi)\sum_{\sigma=\uparrow,\downarrow}\langle(g_{2\sigma}^{\mathrm{AP}}-g_{2\sigma}^{\mathrm{P}})k_\parallel^2\rangle_\sigma\right], \tag{43}$$

where $\mathrm{TMR}=(G_{\mathrm{P}}^{(0)}-G_{\mathrm{AP}}^{(0)})/G_{\mathrm{AP}}^{(0)}$ is the conventional TMR in the absence of SOC, and the functions $g_{1\sigma}^{\mathrm{P}}$, $g_{2\sigma}^{\mathrm{P}}$, $g_{1\sigma}^{\mathrm{AP}}$, and $g_{2\sigma}^{\mathrm{AP}}$ are given by Eqs. (A26), (A27), (A33), and (A34), respectively. Assuming that the spin-orbit effects on the conventional TMR are small one can approximate the ATMR efficiency as

$$\eta \approx \frac{e^2}{hG_{\mathrm{AP}}^{(0)}}\frac{\lambda_\alpha\lambda_\gamma[\cos(2\phi)-1]}{\mathrm{TMR}}\sum_{\sigma=\uparrow,\downarrow}\langle(g_{2\sigma}^{\mathrm{P}}-g_{2\sigma}^{\mathrm{AP}})k_\parallel^2\rangle_\sigma. \tag{44}$$

Note that the angular dependence of the efficiency η is similar to that of the TAMR given in Eq. (34).

It follows from Eq. (43) that when both Bychkov-Rashba and Dresselhaus SOCs are present (i.e., when $\lambda_\alpha\lambda_\gamma \propto \bar{\alpha}\bar{\gamma} \neq 0$), the magnetoresistance becomes anisotropic, resulting in the ATMR effect here predicted. One can see also that this effect exhibits a twofold symmetry with a $\cos(2\phi)$ angular dependence. Unlike the TAMR, when $\bar{\alpha}\bar{\gamma}=0$ the ATMR becomes isotropic but does not vanish. However, in such a limit the efficiency η of the ATMR do vanish [see Eq. (44)], indicating the absence of anisotropy. Like for the TAMR, changes in the sign of $\bar{\alpha}$ result in the inversion (change in sign) of the efficiency η of the ATMR. On the other hand, since the TMR contribution in Eq. (43) is usually the dominant one, the bias-induced changes in the sign of the Bychkov-Rashba parameter $\bar{\alpha}$ will not, in general, cause the inversion (change in sign) of the ATMR. However, the fact that the TMR contribution may change sign in dependence of the applied voltage[48–52] can result in the inversion of the

ATMR. To explain the change in the sign of the conventional TMR (and eventually of the ATMR) when varying the voltage, the detailed band structure has to be considered and the simple parabolic approximation here considered is certainly not sufficient.

We performed calculations within the SSOM of the angular dependence of the ATMR for a Fe/GaAs/Fe MTJ with a fixed value of the Bychkov-Rashba parameter $\alpha_l = 42$ eV Å^2 at the left Fe/GaAs interface. This value was obtained by fitting the theoretical results of Sec. III A to the available experimental data for Fe/GaAs/Au at a bias voltage $V_{\text{bias}} = -90$ mV. We then perform calculations in Fe/GaAs/Fe MTJs with values of α_r slightly different from α_l. The difference between the two interface Bychkov-Rashba SOC parameters may originate from any additional source of interface asymmetry. In practice, for example, the left and right interfaces may not be identical due to imperfections or to a distinct growing technique of the constituents at the interfaces. Another possibility is the different terminations of the semiconductor at the left and right interfaces. For the case of Fe/GaAs/Fe structures, for example, one of the Fe/Gas interface may be Ga terminated while the other may be As terminated.[53,54]

The results for model calculations of ATMR are shown in Figs. 12(a) and 12(b) for the parameters $\alpha_r = 32$ eV Å^2 and $\alpha_r = 52$ eV Å^2. The angular dependence of the ATMR is consistent with Eq. (43). The orientation of the symmetry axis of the ATMR is determined by the sign of the effective value $\bar{\alpha}$. On the other hand, the amplitude of the ATMR shows a behavior opposite to the one corresponding to the TAMR (see Fig. 11), in the sense that now the amplitude of the anisotropy of the TMR is bigger for the case $\alpha_r = 32$ eV Å^2 than for $\alpha_r = 52$ eV Å^2 and, unlike for the case of the TAMR (see Fig. 11), the orientation of the symmetry axis of the ATMR can be flipped by varying the value of α_r.

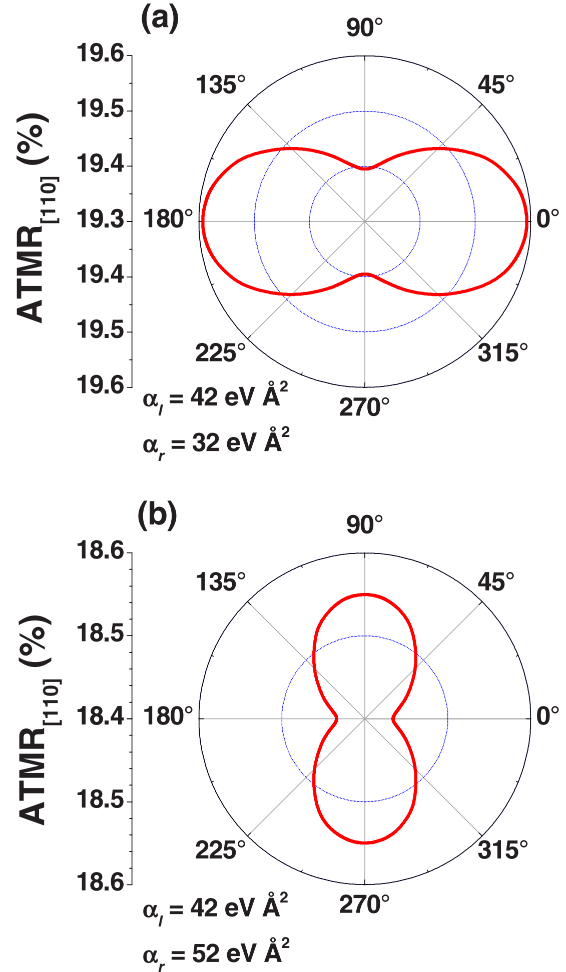

FIG. 12. (Color online) Model calculations of the angular dependence of the ATMR defined in Eq. (41) for a Fe/GaAs/Fe MTJ. (a) For $\alpha_l = 42$ eV Å^2 and $\alpha_r = 32$ eV Å^2 (i.e., $\bar{\alpha} > 0$). (b) For $\alpha_l = 42$ eV Å^2 and $\alpha_r = 52$ eV Å^2 (i.e., $\bar{\alpha} < 0$).

V. PHENOMENOLOGICAL MODEL OF TAMR AND ATMR

In order to explain the origin of the angular dependence of the TAMR [see Eq. (34)] in $F/S/$NM junctions, a phenomenological model based on rather general symmetry considerations was proposed in Ref. 13 and elaborated in more details in Ref. 6. Here we extend this phenomenological model to the case of $F/S/F$ tunnel junctions.

For a given $\mathbf{k}_\parallel$, there are three preferential directions in the system: (i) the magnetization direction $\mathbf{n}_l$ in the left ferromagnet, (ii) the magnetization direction $\mathbf{n}_r$ in the right ferromagnet, and (iii) the direction of the effective SOCF $\mathbf{w}$. A scalar quantity such as the transmissivity T_n corresponding to the nth band can be expanded in a series of the all possible scalars one can form with the vectors $\mathbf{n}_l$, $\mathbf{n}_r$, and $\mathbf{w}$. Thus, to the second order in $|\mathbf{w}|$, we have

$$T_n = T_n^{(0)} + T_n^{(1)} + T_n^{(2)}. \tag{45}$$

The zero-order terms have the general form

$$T_n^{(0)} = a_{1n}^{(0)} + a_{2n}^{(0)}(\mathbf{n}_l \cdot \mathbf{n}_r), \tag{46}$$

where $a_{1n}^{(0)}$ and $a_{2n}^{(0)}$ are expansion coefficients.

Taking into account that $\mathbf{n}_l = [\cos(\phi + \pi/4), \sin(\phi + \pi/4), 0]$ and $\mathbf{n}_r = [\cos(\theta + \phi + \pi/4), \sin(\theta + \phi + \pi/4), 0]$, the general angular dependence of $T_n^{(0)}$ can be extracted from Eq. (46). The result is

$$T_n^{(0)} = a_{1n}^{(0)} + a_{2n}^{(0)} \cos(\theta). \tag{47}$$

This equation describes the dependence of the transmissivity on the relative angle θ between the magnetizations in the left and right ferromagnetic electrodes in the absence of SOC and is consistent with previous results.[3,6]

The first- and second-order contributions can be cast in the following general forms:

$$T_n^{(1)} = a_{1n}^{(1)}(\mathbf{n}_l \cdot \mathbf{w}) + a_{2n}^{(1)}(\mathbf{n}_r \cdot \mathbf{w})^2 \tag{48}$$

and

$$T_n^{(2)} = [a_{1n}^{(2)} + a_{2n}^{(2)}(\mathbf{n}_l \cdot \mathbf{n}_r)]|\mathbf{w}|^2 + a_{3n}^{(2)}|(\mathbf{n}_l \cdot \mathbf{w})|^2 + a_{4n}^{(2)}|(\mathbf{n}_r \cdot \mathbf{w})|^2 + a_{5n}^{(2)}(\mathbf{n}_l \cdot \mathbf{w})(\mathbf{n}_r \cdot \mathbf{w}), \tag{49}$$

respectively.

All the expansion coefficients $a_{in}^{(j)}$ $(i=1,2,\ldots 5;\ j=0,1,2)$ present in Eqs. (46)–(49) are related to the system in the absence of the SOC. Therefore, they do not depend on the magnetization orientation(s). These coefficients should also reflect the cubic symmetry of the involved bulk structures. In particular, they must obey the relations $a_{in}^{(j)}(k_x,k_y)=a_{in}^{(j)}(-k_x,-k_y)$, $a_{in}^{(j)}(k_x,k_y)=a_{in}^{(j)}(-k_x,k_y)$, and $a_{in}^{(j)}(k_x,k_y)=a_{in}^{(j)}(k_y,k_x)$.

To second order in the SOC, the conductance is then given by

$$G=\frac{e^2}{h}\sum_n (\langle T_n^{(0)}\rangle+\langle T_n^{(2)}\rangle), \tag{50}$$

where $\langle\ldots\rangle$ denotes average over $\mathbf{k}_\parallel$ and energy E for all the available transport channels. Note that because of the above-mentioned symmetry properties of the expansion coefficients and the fact that the effective SOCF must be an odd function of $\mathbf{k}$, the first-order contribution vanishes after averaging. From similar symmetry considerations and taking into account Eqs. (47), (49), and (50) one can identify which contributions vanish after averaging. Dropping these contributions the remaining general form of the total conductance is

$$G(\theta,\phi)=G_1+G_2\cos(\theta)+G_3\cos(2\phi)+G_4\cos(2\phi+2\theta)+G_5\cos(2\phi+\theta), \tag{51}$$

where

$$G_1=\frac{e^2}{h}\sum_n\left\langle a_{1n}^{(0)}+\frac{|\mathbf{w}|^2}{2}(2a_{1n}^{(2)}+a_{3n}^{(2)}+a_{4n}^{(2)})\right\rangle, \tag{52}$$

$$G_2=\frac{e^2}{h}\sum_n\left\langle a_{2n}^{(0)}+\frac{|\mathbf{w}|^2}{2}(2a_{2n}^{(2)}+a_{5n}^{(2)})\right\rangle, \tag{53}$$

$$G_3=\frac{e^2}{h}\sum_n\langle a_{3n}^{(2)}w_xw_y\rangle, \tag{54}$$

$$G_4=\frac{e^2}{h}\sum_n\langle a_{4n}^{(2)}w_xw_y\rangle, \tag{55}$$

and

$$G_5=\frac{e^2}{h}\sum_n\langle a_{5n}^{(2)}w_xw_y\rangle. \tag{56}$$

The next higher-order contributions in the expansion in Eq. (45) which do not vanish after averaging contain terms of the fourth order in the SOCF, which lead to an extra fourfold contribution to the anisotropy, and terms of fourth order in the cosine directions of $\mathbf{n}_l$ and $\mathbf{n}_r$ which describe the fourfold anisotropy inherent to the bulk of the involved structures. These contributions can in principle be incorporated in the proposed phenomenological model. However, for the sake of simplicity and taking into account that in the experiments in Fe/GaAs based MTJs no traces of any fourfold or higher-order contributions to the TAMR are observed, it is reasonable to expect that higher-order contributions are small and can be neglected in modeling. Apart from this assumption, no other approximation has been made throughout our discussion; the equations above are quite general. They are valid up to the second order in the strength of the SOCF regardless of the specific form of $\mathbf{w}$ and the details of the band structure. The information of the specific band structure of the actual system is encoded in the expansion coefficients. Naturally, unless further approximations are made (such as the ones assumed in the previous sections), the detailed $\mathbf{k}$ dependence of these coefficients has to be extracted from first-principles calculations. However, for our purpose in this section, in which the coefficients are introduced phenomenologically, it is enough to know symmetry properties. This explains why the angular dependence of the TAMR experimentally observed in Fe/GaAs/Au MTJs appears to be quite regular and relatively simple[13] in spite of the high complexity of the band structure of such a system.

One can see that for the case of a $F/S/$NM junction or for the case of parallel and antiparallel configurations in a $F/S/F$ junction, the general angular dependence given in Eq. (51) is consistent with the corresponding expressions obtained in Appendix A. We want to stress, however, that the relations presented in Appendix A are the result of a specific approximation (the DDFM), while Eqs. (51)–(56) as discussed above are more general.

In what follows we consider the case of a SOCF of the Bychkov-Rashba+Dresselhaus form [see Eq. (11)]. Thus, in the in-plane configuration here considered $\mathbf{n}_l$, $\mathbf{n}_r$, and $\mathbf{w}$ lie in a plane parallel to the layers. More general relations corresponding to arbitrary orientations of $\mathbf{n}_l$, $\mathbf{n}_r$, and $\mathbf{w}$ will be given elsewhere.[55]

The general form of the TAMR in $F/S/$NM junctions follows from Eqs. (11), (29), and (51). Proceeding as in Sec. III A one finds

$$\mathrm{TAMR}_{[110]}(\phi)\approx\frac{e^2}{h}\frac{1}{G^{(0)}}\left[\sum_n\langle-(a_{3n}^{(2)}+a_{4n}^{(2)}+a_{5n}^{(2)})k_\parallel^2\rangle\right]\times\lambda_\alpha\lambda_\gamma[\cos(2\phi)-1], \tag{57}$$

which is consistent with the corresponding expression found within the DDFM [see Eq. (34)].

In the previous sections we identified the voltage-induced change in the sign of the effective Bychkov-Rashba SOC parameter $\bar{\alpha}\propto\lambda_\alpha$ as a possible mechanism leading to the change in the sign of the TAMR. This possibility results from Eq. (57). However, a similar effect could be obtained if the sign of the first term within the square brackets in Eq. (57) were bias dependent. In our previous model calculations [see Refs. 6 and 13] we found that within the voltages used in the experiments such a term is almost bias independent. It is not known, however, whether such a behavior constitutes a general trend or is just an artifact of our simplified model. Certainly, first-principles investigations about the mechanisms leading to the inversion of the TAMR in Fe/GaAs based MTJs are needed.

Similarly, one obtains for the TMR and ATMR in $F/S/F$ junctions the following general expressions:

$$\mathrm{TMR} = \frac{e^2}{h}\frac{1}{G_{\mathrm{AP}}^{(0)}}\sum_n \langle 2a_{2n}^{(0)}k_{\parallel}^2\rangle \tag{58}$$

and

$$\mathrm{ATMR}_{[110]}(\phi) = \mathrm{TMR} + \frac{e^2}{2h}\frac{(\lambda_\alpha^2+\lambda_\gamma^2)}{G_{\mathrm{AP}}^{(0)}}\sum_n \langle(4a_{2n}^{(2)}+2a_{5n}^{(2)})k_{\parallel}^2\rangle + \frac{e^2}{h}\frac{1}{G_{\mathrm{AP}}^{(0)}}\left[\sum_n \langle 2a_{4n}^{(2)}k_{\parallel}^2\rangle\right]\lambda_\alpha\lambda_\gamma\cos(2\phi), \tag{59}$$

respectively. Note that Eq. (59) is consistent with our previous result in Eq. (43).

The TAMR in a $F/S/F$ exhibits a more complicated angular dependence, which has the general form

$$\mathrm{TAMR}_{[110]}(\theta,\phi) = \frac{A(\theta)[1-\cos(2\phi)]+B(\theta)\sin(2\phi)}{G_1+G_2\cos\theta+A(\theta)\cos(2\phi)-B(\theta)\sin(2\phi)}, \tag{60}$$

where

$$A(\theta) = G_3 + G_4\cos(2\theta) + G_5\cos\theta \tag{61}$$

and

$$B(\theta) = G_4\sin(2\theta) + G_5\sin\theta. \tag{62}$$

At the phenomenological level, the expansion constants $G_1,\ldots G_5$ in Eqs. (51) and (60) can be determined from conductance measurements (or conductance theoretical evaluation) at selected values of θ and ϕ. For example, the values of the phenomenological constants can be determined as follows:

$$G_1 = \frac{G(\pi/2,0)+G(\pi/2,\pi/2)}{2}, \tag{63}$$

$$G_2 = G(0,\pi/4) - G_1, \tag{64}$$

$$G_5 = G_1 - G(\pi/2,\pi/4), \tag{65}$$

$$G_3 = G(\pi/4,0) - G_1 - \frac{\sqrt{2}}{2}(G_2+G_5), \tag{66}$$

and

$$G_4 = G_1 + G_3 - G(\pi/2,0). \tag{67}$$

It is worth noting that although we have referred to the coefficients $G_1,\ldots,G_5$ as constants, strictly speaking, these parameters may exhibit a dependence on the relative angle θ. Such a dependence may originate from the fact that the averages containing the components of the SOCF [see Eqs. (52)–(56)] are, in principle, θ dependent. However, as shown below, this effect is weak for the system here considered.

In order to check the validity of the general angular dependence given in Eqs. (51) and (60) we have computed the expansion coefficients from Eqs. (63)–(67) by using the SSOM. We then evaluate the TAMR by using the phenomenological relation given in Eq. (60) and compare the results (see dashed lines in Fig. 11) with the full angular dependence obtained from the SSOM (solid lines in Fig. 11). The agreement is satisfactory although some small discrepancies appear. We attribute these discrepancies to the fact that when determining the coefficients $G_1,\ldots,G_5$ from Eqs. (63)–(67) we have ignored, as discussed above, that these coefficients are weakly θ dependent.

VI. CONCLUSIONS

We have investigated the spin-orbit-induced anisotropy of the tunneling magnetoresistance of $F/S/$NM and $F/S/F$ MTJs. By performing model calculations we have shown that the twofold symmetry of the TAMR effect may arise from the interplay of Bychkov-Rashba and Dresselhaus SOCs. The spin-orbit interference effects in $F/S/F$ MTJs lead to the anisotropy of the conventional TMR. Thus, the ATMR depends on the absolute magnetization directions in the ferromagnets. The magnetoresistance dependence on the absolute orientation of the magnetization in the ferromagnets is deduced from general symmetry considerations.

ACKNOWLEDGMENTS

We are grateful to M. Gmitra for useful hints and discussions and to D. Weiss and J. Moser for discussions on TAMR related experiments. This work was supported by the Deutsche Forschungsgemeinschaft (DFG) through the Sonderforschungsbereich (SFB) 689.

APPENDIX A

The eigenfunctions of the Hamiltonian given by Eq. (7) obey the following matching conditions:

$$\Psi_\sigma^{(l)}(0^-) = \Psi_\sigma^{(r)}(0^+);$$

$$\frac{\hbar^2}{2m_0}\left.\frac{d\Psi_\sigma^{(l)}}{dz}\right|_{z=0^-} + (V_0 d + \mathbf{w}\cdot\boldsymbol{\sigma})\Psi_\sigma^{(l)}(0^-) = \frac{\hbar^2}{2m_0}\left.\frac{d\Psi_\sigma^{(r)}}{dz}\right|_{z=0^+}, \tag{A1}$$

which, with the scattering states in Eqs. (12) and (13), lead to a system of four linear equations for determining the coefficients $r_{\sigma,\sigma}$, $r_{\sigma,-\sigma}$, $t_{\sigma,\sigma}$, and $t_{\sigma,-\sigma}$. The transmission coefficients are found to be given by

$$t_{\sigma,\sigma} = -\frac{4d^2\sqrt{k_\sigma}(k_{-\sigma}+\kappa_{-\sigma}+iQ)(1+e^{i(\phi_r-\phi_l)})}{\Omega} + \frac{8id\sqrt{k_\sigma}(\mathbf{U}\cdot\mathbf{S}_{\sigma,\sigma})}{\Omega} \tag{A2}$$

and

$$t_{\sigma,-\sigma} = \frac{4d\sqrt{k_\sigma}d(k_{-\sigma}+\kappa_\sigma+iQ)(1-e^{i(\phi_r-\phi_l)})}{\Omega} - \frac{8i(\mathbf{U}\cdot\mathbf{S}_{\sigma,-\sigma})}{\Omega}, \tag{A3}$$

where

$$\Omega = \Omega_+(-)\Omega_-(+) - \Omega_+(+)\Omega_-(-), \tag{A4}$$

with

$$\Omega_\pm(\lambda) = d(k_{\pm\sigma} + \kappa_{\lambda\sigma} + iQ)(1 \pm \lambda e^{i(\phi_r - \phi_l)}) + 2i(\mathbf{U}\cdot\mathbf{S}_{\pm\sigma,\lambda\sigma}). \tag{A5}$$

The vectors $\mathbf{S}_{\sigma,\sigma'}$ ($\sigma' = \pm\sigma$) are given by

$$\mathbf{S}_{\sigma,\sigma'} = \chi_\sigma^{(l)\dagger}\boldsymbol{\sigma}\chi_{\sigma'}^{(r)}, \tag{A6}$$

while $Q = 2m_0V_0d/\hbar^2$ and $\mathbf{U} = (2m_0d/\hbar^2)\mathbf{w}$. The transmissivity for an incident particle with spin σ is given by Eq. (17). For the case of a $F/S/$NM junction we can approximate $\kappa = \kappa_\sigma \approx \kappa_{-\sigma}$ and the transmissivity reduces to

$$T_\sigma = \mathrm{Re}[\kappa(|t_{\sigma,\sigma}|^2 + |t_{\sigma,-\sigma}|^2)]. \tag{A7}$$

In order to obtain a simplified analytical expression for the TAMR in $F/S/$NM junctions, we consider the case in which the effective SOCF is small. In such a case one can expand Eq. (A7) in powers of $w = |\mathbf{w}|$ and obtain the conductance from Eq. (28). The result, up to second order in w, reads as

$$G_\sigma \approx G_\sigma^{\mathrm{iso}} + G_\sigma^{\mathrm{aniso}}. \tag{A8}$$

The isotropic part of the conductance is given by

$$G_\sigma^{\mathrm{iso}} = G_\sigma^{(0)} + G'_\sigma, \tag{A9}$$

where

$$G_\sigma^{(0)} = \frac{e^2}{h}\left\langle \frac{4|k_{F,\sigma}|\kappa_F}{|A_\sigma|^2} \right\rangle_\sigma, \tag{A10}$$

with

$$A_{\pm\sigma} = k_{F,\pm\sigma} + \kappa_F + iQ \tag{A11}$$

as the conductance in absence of the SOC and

$$G'_\sigma = -\frac{e^2}{2h}(\lambda_\alpha^2 + \lambda_\gamma^2)\langle g_{1\sigma}k_\parallel^2\rangle_\sigma \tag{A12}$$

as the isotropic contribution induced by the SOC. Here we have denoted $k_{F\sigma} = k_\sigma(E_F, k_\parallel)$, $\kappa_F = \kappa(E_F, k_\parallel)$, and

$$g_{1\sigma} = \frac{8\kappa_F|k_{F,\sigma}|}{|A_\sigma|^2|A_{-\sigma}|^2}\left(\frac{2\,\mathrm{Re}[A_\sigma A_{-\sigma}]}{|A_\sigma|^2} - 1\right) - g_{2\sigma}. \tag{A13}$$

We have also introduced dimensionless SOC parameters as

$$\lambda_\alpha = \frac{2m_0}{\hbar^2}\bar{\alpha}, \lambda_\gamma = \frac{2m_0}{\hbar^2}\bar{\gamma}. \tag{A14}$$

The function g_2 is defined below in Eq. (A18). The average

$$\langle\ldots\rangle_\sigma = \frac{1}{2\pi}\int_0^{k_{\max}^\sigma} \ldots k_\parallel dk_\parallel, \tag{A15}$$

where

$$k_{\max}^\sigma = \min\left[\sqrt{\frac{2m_0}{\hbar^2}\left(E_F + \sigma\frac{\Delta_l}{2}\right)}, \quad \sqrt{\frac{2m_0}{\hbar^2}E_F}\right] \tag{A16}$$

denotes the maximum values of $k_\parallel$ for which we have incident and transmitted propagating states. In the average defined in Eq. (A15) the corresponding angular integration over $\mathbf{k}_\parallel$ [see Eq. (28)] has already been performed.

The spin-orbit-induced anisotropy of the conductance is determined by the relation

$$G_\sigma^{\mathrm{aniso}}(\phi) = -\frac{e^2}{h}\lambda_\alpha\lambda_\gamma\langle g_{2\sigma}k_\parallel^2\rangle_\sigma \cos(2\phi), \tag{A17}$$

where

$$g_{2\sigma} = \frac{4\kappa_F|k_{F,\sigma}|\{|A_{-\sigma}|^2|A_\sigma - A_{-\sigma}|^2 - 4\,\mathrm{Im}[A_{-\sigma}][|A_{-\sigma}|^2\,\mathrm{Im}(A_\sigma) - |A_\sigma|^2\,\mathrm{Im}(A_{-\sigma})]\}}{|A_\sigma|^4|A_{-\sigma}|^4}. \tag{A18}$$

The total conductance can then be written as

$$G(\phi) \approx G^{\mathrm{iso}} + G^{\mathrm{aniso}}(\phi), \tag{A19}$$

with $G^{\mathrm{iso}} = G_\uparrow^{\mathrm{iso}} + G_\downarrow^{\mathrm{iso}}$ and $G^{\mathrm{aniso}}(\phi) = G_\uparrow^{\mathrm{aniso}}(\phi) + G_\downarrow^{\mathrm{aniso}}(\phi)$.

We now consider the case of a $F/S/F$ tunnel junction. For the general case of arbitrary orientations of the magnetization in the left and right ferromagnets, the analytical expressions for the conductance are very lengthy, and we therefore omit them here. Simpler expressions are found, however, for the particular cases of parallel (P) and antiparallel (AP) configurations. If we consider that the ferromagnetic electrodes are made of the same material, then $k_\sigma = \kappa_\sigma$ and the transmissivity reduces to

$$T_\sigma = \mathrm{Re}[k_\sigma|t_{\sigma,\sigma}|^2 + k_{-\sigma}|t_{\sigma,-\sigma}|^2]. \tag{A20}$$

Following the same procedure as above, the following expression for the conductance in the parallel configuration is found

$$G_{\mathrm{P}} \approx G_{\mathrm{P}}^{\mathrm{iso}} + G_{\mathrm{P}}^{\mathrm{aniso}}(\phi). \tag{A21}$$

The isotropic part is given by

$$G_{\mathrm{P}}^{\mathrm{iso}} = G_{\mathrm{P}}^{(0)} + G'_{\mathrm{P}}, \tag{A22}$$

where

$$G_{\mathrm{P}}^{(0)}=\frac{e^2}{h}\sum_{\sigma=\uparrow,\downarrow}\left\langle\frac{4k_{F,\sigma}^2}{4k_{F,\sigma}^2+Q^2}\right\rangle_\sigma, \tag{A23}$$

and

$$G_{\mathrm{P}}'=-\frac{e^2}{2h}(\lambda_\alpha^2+\lambda_\gamma^2)\sum_{\sigma=\uparrow,\downarrow}\langle g_{1\sigma}^{\mathrm{P}}k_\parallel^2\rangle_\sigma. \tag{A24}$$

The anisotropic contribution reads as

$$G_{\mathrm{P}}^{\mathrm{aniso}}(\phi)=\frac{e^2}{h}\lambda_\alpha\lambda_\gamma\sum_{\sigma=\uparrow,\downarrow}\langle g_{2\sigma}^{\mathrm{P}}k_\parallel^2\rangle_\sigma\cos(2\phi). \tag{A25}$$

The functions $g_{1\sigma}^{\mathrm{P}}$ and $g_{2\sigma}^{\mathrm{P}}$ are given by

$$g_{1\sigma}^{\mathrm{P}}=\frac{8k_{F,\sigma}(2k_{F,\sigma}+k_{F,-\sigma})Q^2-32k_{F,\sigma}^3k_{F,-\sigma}}{(4k_{F,\sigma}^2+Q^2)^2(4k_{F,-\sigma}^2+Q^2)}-g_{2\sigma}^{\mathrm{P}} \tag{A26}$$

and

$$g_{2\sigma}^{\mathrm{P}}=\frac{4k_{F,\sigma}(k_{F,-\sigma}-k_{F,\sigma})}{(4k_{F,\sigma}^2+Q^2)^3(4k_{F,-\sigma}^2+Q^2)}\times[16k_{F,-\sigma}k_{F,\sigma}^3-12k_{F,\sigma}(k_{F,\sigma}+k_{F,-\sigma})Q^2+Q^4], \tag{A27}$$

respectively.

On the other hand, for the case of antiparallel configuration one obtains the following expressions:

$$G_{\mathrm{AP}}\approx G_{\mathrm{AP}}^{\mathrm{iso}}+G_{\mathrm{AP}}^{\mathrm{aniso}}(\phi), \tag{A28}$$

where

$$G_{\mathrm{AP}}^{\mathrm{iso}}=G_{\mathrm{AP}}^{(0)}+G_{\mathrm{AP}}', \tag{A29}$$

$$G_{\mathrm{AP}}^{(0)}=\frac{e^2}{h}\sum_{\sigma=\uparrow,\downarrow}\left\langle\frac{4k_{F,\sigma}(k_{F,-\sigma}-k_{F,\sigma})}{(k_{F,-\sigma}+k_{F,\sigma})^2+Q^2}\right\rangle_\sigma, \tag{A30}$$

and

$$G_{\mathrm{AP}}'=-\frac{e^2}{2h}(\lambda_\alpha^2+\lambda_\gamma^2)\sum_{\sigma=\uparrow,\downarrow}\langle g_{1\sigma}^{\mathrm{AP}}k_\parallel^2\rangle_\sigma. \tag{A31}$$

The anisotropic contribution for the antiparallel case reads as

$$G_{\mathrm{AP}}^{\mathrm{aniso}}(\phi)=\frac{e^2}{h}\lambda_\alpha\lambda_\gamma\sum_{\sigma=\uparrow,\downarrow}\langle g_{2\sigma}^{\mathrm{AP}}k_\parallel^2\rangle_\sigma\cos(2\phi), \tag{A32}$$

and the functions $g_{1\sigma}^{\mathrm{AP}}$ and $g_{2\sigma}^{\mathrm{AP}}$ are given by

$$g_{1\sigma}^{\mathrm{AP}}=\frac{8k_{F,\sigma}(2k_{F,-\sigma}+k_{F,\sigma})Q^2}{[(k_{F,\sigma}+k_{F,-\sigma})^2+Q^2]^3}-g_{2\sigma}^{\mathrm{AP}}+\frac{8k_{F,\sigma}(k_{F,\sigma}-2k_{F,-\sigma})(k_{F,\sigma}+k_{F,-\sigma})^2}{[(k_{F,\sigma}+k_{F,-\sigma})^2+Q^2]^3} \tag{A33}$$

and

$$g_{2\sigma}^{\mathrm{AP}}=\frac{4k_{F,\sigma}(k_{F,\sigma}-k_{F,-\sigma})}{[(k_{F,\sigma}+k_{F,-\sigma})^2+Q^2]^2}, \tag{A34}$$

respectively.

In the derivation of Eqs. (A24), (A25), (A31), and (A32) we assumed that the spin-orbit parameters $\bar{\alpha}$ and $\bar{\gamma}$ are independent of the relative magnetization orientations in the ferromagnets. Strictly speaking the values of $\bar{\alpha}$ and $\bar{\gamma}$ are θ dependent and therefore to the parallel and antiparallel configurations correspond slightly different sets of effective spin-orbit parameters. This effect turns out to be negligible for the system here investigated, and we therefore omit it.

In both the parallel and antiparallel cases, the averages have the same meaning as in Eq. (A15) but now with $k_{\max}^\sigma$ defined as

$$k_{\max}^\sigma=\sqrt{\frac{2m_0}{\hbar^2}\left(E_F+\sigma\frac{\Delta_l}{2}\right)}. \tag{A35}$$

APPENDIX B

Here we discuss the details about the solutions of the SSOM and provide approximate expressions for the tunneling coefficients.

By requiring the probability flux conservation across the interfaces one obtains that the eigenfunctions of the Hamiltonian in Eq. (18) should fulfill the following boundary conditions:

$$\Psi_\sigma^{(i)}(z_{ij})=\Psi_\sigma^{(j)}(z_{ij}), \tag{B1}$$

$$\frac{\hbar^2}{2m_i}\left[1-\frac{2m_i\gamma_i}{\hbar}(k_x\sigma_x-k_y\sigma_y)\right]\frac{d\Psi_\sigma^{(i)}}{dz}\bigg|_{z=z_{ij}}-\frac{\hbar^2}{2m_j}\left[1-\frac{2m_j\gamma_j}{\hbar}(k_x\sigma_x-k_y\sigma_y)\right]\frac{d\Psi_\sigma^{(j)}}{dz}\bigg|_{z=z_{ij}}=-\alpha_{ij}(k_x\sigma_y-k_y\sigma_x)\Psi_\sigma^{(i)}(z_{ij}), \tag{B2}$$

where $i,j=l,c,r$ and $z_{lc}=0$ and $z_{cr}=d$ are the locations of the left and right interfaces, respectively. The interface Bychkov-Rashba parameters are introduced as $\alpha_{lc}=\alpha_l$ and $\alpha_{cr}=-\alpha_r$, while the Dresselhaus parameter is $\gamma_c=\gamma$ in the semiconductor and vanishes elsewhere (i.e., $\gamma_l=\gamma_r=0$).

Applying the above boundary conditions to the scattering states given in Sec. II B one obtains a system of eight linear equations for determining the eight unknown expansion coefficients. The exact expressions for the transmission coefficients $t_{\sigma,\sigma}$ and $t_{\sigma,-\sigma}$ are quite cumbersome. However, simplified analytical expressions for $t_{\sigma,\sigma}$ and $t_{\sigma,-\sigma}$ are found in the limit $q_0d\gg1$. In such a case one finds the following approximate relations for the tunneling coefficients:

$$t_{\sigma,\sigma}=-\frac{D_{\sigma,\sigma}}{D},\quad t_{\sigma,-\sigma}=\frac{D_{\sigma,-\sigma}}{D}, \tag{B3}$$

where $D=f_-(-)f_+(-)-f_-(+)f_+(+)$, with

$$f_\pm(\lambda)=\pm\frac{i\alpha_rk_\parallel Q}{2V_0}(\sigma e^{i(\phi_r-\xi+\pi/4)}+\lambda e^{2i\xi})+\frac{d}{2}\left(\frac{m_0}{m_{\pm\lambda}}q_{\mp\lambda}-i\kappa_{\pm\sigma}\right)(1-\lambda\sigma e^{i(\phi_r+\xi+\pi/4)}) \tag{B4}$$

and

$$\frac{1}{m_{\pm}} = \frac{1}{m_c}\left(1 \pm \frac{2m_c\gamma k_{\parallel}}{\hbar^2}\right). \tag{B5}$$

Furthermore, we have

$$D_{\sigma,\sigma} = \frac{2m_0 d}{m_+}q_- f_-(+)g_- - \frac{2m_0 d}{m_-}q_+ f_-(-)g_+, \tag{B6}$$

and

$$D_{\sigma,-\sigma} = \frac{2m_0 d}{m_+}q_- f_+(-)g_- - \frac{2m_0 d}{m_-}q_+ f_+(+)g_+. \tag{B7}$$

In these equations we introduced the notation

$$g_{\pm} = \frac{id\sqrt{k_\sigma}\left[\left(f_0 \mp h_1 - \frac{m_0 d}{m_{\pm}}q_{\mp}\right)(1 \pm \sigma e^{i(\phi_l+\xi+\pi/4)}) \mp h_2(1 \mp \sigma e^{i(\phi_l+\xi+\pi/4)})\right]e^{-q_{\pm}d}}{h_2^2 + \left(f_0 - h_1 - \frac{m_0 d}{m_+}q_-\right)\left(f_0 + h_1 - \frac{m_0 d}{m_-}q_+\right)}, \tag{B8}$$

where $f_0 = i(k_\sigma + k_{-\sigma})d/2$,

$$h_1 = \frac{i\sigma d}{2}(k_\sigma - k_{-\sigma})\cos(\phi_l + \xi + \pi/4) + \frac{\alpha_l k_{\parallel} Q}{V_0}\sin(2\xi), \tag{B9}$$

and

$$h_2 = -\frac{\sigma d}{2}(k_\sigma - k_{-\sigma})\sin(\phi_l + \xi + \pi/4) - i\frac{\alpha_l k_{\parallel} Q}{V_0}\cos(2\xi). \tag{B10}$$

It is worth noting that the approximate expressions for the tunneling coefficients here provided are valid up to first order in $\exp(-q_{\pm}d)$. This approximation is appropriate for treating junctions with high and not too thin potential barriers. For the systems here considered the height of the barrier (with respect to the Fermi level) is about $V_b = (V_0 - E_F) \approx 0.75$ eV and d varies from 20 to 200 Å. In such cases the approximations here discussed turns out to be excellent.

It is not difficult to show that in the limit $\alpha_l = \alpha_r = \gamma = 0$, the expressions for the tunneling coefficients here obtained reduce to the ones reported in Ref. 6 for the case of vanishing SOC.

We also remark that the expressions above were obtained for the general case of a $F/S/F$ tunnel junction but the corresponding expressions for a $F/S/$NM junction can easily be obtained by taking the limits $\kappa_\sigma = \kappa_{-\sigma} = \kappa$ and $\phi_l = \phi_r = \phi$.

[1] M. Jullierè, Phys. Lett. **54A**, 225 (1975).
[2] J. S. Moodera, L. R. Kinder, T. M. Wong, and R. Meservey, Phys. Rev. Lett. **74**, 3273 (1995).
[3] J. C. Slonczewski, Phys. Rev. B **39**, 6995 (1989).
[4] S. Maekawa, S. Takahashi, and H. Imamura, in *Spin Dependent Transport in Magnetic Nanostructures*, edited by S. Maekawa and T. Shinjo (Taylor and Francis, New York, 2002), pp. 143–236.
[5] I. Žutić, J. Fabian, and S. Das Sarma, Rev. Mod. Phys. **76**, 323 (2004).
[6] J. Fabian, A. Matos-Abiague, C. Ertler, P. Stano, and I. Žutić, Acta Phys. Slov. **57**, 565 (2007).
[7] M. Tanaka and Y. Higo, Phys. Rev. Lett. **87**, 026602 (2001).
[8] Y. Higo, H. Shimizu, and M. Tanaka, J. Appl. Phys. **89**, 6745 (2001).
[9] C. Gould, C. Rüster, T. Jungwirth, E. Girgis, G. M. Schott, R. Giraud, K. Brunner, G. Schmidt, and L. W. Molenkamp, Phys. Rev. Lett. **93**, 117203 (2004).
[10] C. Rüster, C. Gould, T. Jungwirth, J. Sinova, G. M. Schott, R. Giraud, K. Brunner, G. Schmidt, and L. W. Molenkamp, Phys. Rev. Lett. **94**, 027203 (2005).
[11] H. Saito, S. Yuasa, and K. Ando, Phys. Rev. Lett. **95**, 086604 (2005).
[12] L. Brey, C. Tejedor, and J. Fernández-Rossier, Appl. Phys. Lett. **85**, 1996 (2004).
[13] J. Moser, A. Matos-Abiague, D. Schuh, W. Wegscheider, J. Fabian, and D. Weiss, Phys. Rev. Lett. **99**, 056601 (2007).
[14] M. N. Khan, J. Henk, and P. Bruno, J. Phys.: Condens. Matter **20**, 155208 (2008).
[15] B. G. Park, J. Wunderlich, D. A. Williams, S. J. Joo, K. Y. Jung, K. H. Shin, K. Olejník, A. B. Shick, and T. Jungwirth, Phys. Rev. Lett. **100**, 087204 (2008).
[16] D. Chiba, F. Matsukura, and H. Ohno, Physica E **21**, 966 (2004).
[17] P. Sankowski, P. Kacman, J. A. Majewski, and T. Dietl, Phys. Rev. B **75**, 045306 (2007).
[18] A. L. Efros and B. I. Shklovskii, J. Phys. C **8**, L49 (1975).
[19] R. Giraud, M. Gryglas, L. Thevenard, A. Lemaître, and G. Faini, Appl. Phys. Lett. **87**, 242505 (2005).
[20] M. Ciorga, M. Schlapps, A. Einwanger, S. Geißler, J. Sadowski, W. Wegscheider, and D. Weiss, New J. Phys. **9**, 351 (2007).

[21] K. I. Bolotin, F. Kuemmeth, and D. C. Ralph, Phys. Rev. Lett. **97**, 127202 (2006).
[22] J. D. Burton, R. F. Sabirianov, J. P. Velev, O. N. Mryasov, and E. Y. Tsymbal, Phys. Rev. B **76**, 144430 (2007).
[23] A. D. Giddings *et al.*, Phys. Rev. Lett. **94**, 127202 (2005).
[24] D. Jacob, J. Fernández-Rossier, and J. J. Palacios, Phys. Rev. B **77**, 165412 (2008).
[25] L. Gao, X. Jiang, S. H. Yang, J. D. Burton, E. Y. Tsymbal, and S. S. P. Parkin, Phys. Rev. Lett. **99**, 226602 (2007).
[26] R. S. Liu, L. Michalak, C. M. Canali, L. Samuelson, and H. Pettersson, Nano Lett. **8**, 848 (2008).
[27] A. N. Chantis, K. D. Belashchenko, E. Y. Tsymbal, and M. van Schilfgaarde, Phys. Rev. Lett. **98**, 046601 (2007).
[28] A. B. Shick, F. Máca, J. Mašek, and T. Jungwirth, Phys. Rev. B **73**, 024418 (2006).
[29] A. B. Shick, F. Máca, M. Ondráček, O. N. Mryasov, and T. Jungwirth, Phys. Rev. B **78**, 054413 (2008).
[30] M. Trushin and J. Schliemann, Phys. Rev. B **75**, 155323 (2007).
[31] J. L. Cheng, M. W. Wu, and I. C. da Cunha Lima, Phys. Rev. B **75**, 205328 (2007).
[32] O. Chalaev and D. Loss, Phys. Rev. B **77**, 115352 (2008).
[33] N. S. Averkiev and L. E. Golub, Phys. Rev. B **60**, 15582 (1999).
[34] P. Stano and J. Fabian, Phys. Rev. Lett. **96**, 186602 (2006).
[35] S. M. Badalyan, A. Matos-Abiague, G. Vignale, and J. Fabian, arXiv:0804.3366 (unpublished).
[36] G. Dresselhaus, Phys. Rev. **100**, 580 (1955).
[37] U. Rössler and J. Kainz, Solid State Commun. **121**, 313 (2002).
[38] R. Winkler, *Spin-Orbit Coupling Effects in Two-Dimensional Electron and Hole Systems* (Springer, Berlin, 2003).
[39] Y. A. Bychkov and E. I. Rashba, J. Phys. C **17**, 6039 (1984).
[40] S. D. Ganichev *et al.*, Phys. Rev. Lett. **92**, 256601 (2004).
[41] W. Zawadzki and P. Pfeffer, Semicond. Sci. Technol. **19**, R1 (2004).
[42] Equation (22) can be well justified at semiconductor interfaces.[56] We propose it here as a phenomenological model for metal/semiconductor interfaces, as the simplest description of the interface-induced silicon-on-insulator (SOI) symmetry. For metallic surfaces the Bychkov-Rashba SOI has already been investigated.[57,58] We assume that electrons with small transverse momenta p_x and p_y have sizable tunneling probabilities, justifying the linear character of the SOI.
[43] In general, an additional voltage dependence of the transmissivity may originate from the voltage dependence of the Dresselhaus parameter. Such a dependence is weak in semiconductors and is neglected in our model.
[44] M. Gmitra, A. Matos-Abiague, C. Ambrosch-Draxl, and J. Fabian (unpublished).
[45] Note also that when the effective Bychkov-Rashba parameter $\bar{\alpha}$ changes sign, the axes of symmetry of $|\mathbf{w}|$ are flipped by 90° and the situation above explained is reversed (i.e., now the transmission corresponding to the magnetization direction [110] becomes the dominant one), leading to the inversion of the TAMR effect.
[46] J. Wang, D. Y. Xing, and H. B. Sun, J. Phys.: Condens. Matter **15**, 4841 (2003).
[47] N. W. Ashcroft and N. D. Mermin, *Solid State Physics* (Saunders, Philadelphia, 1976).
[48] J. M. De Teresa, A. Barthelemy, A. Fert, J. P. Contour, R. Lyonnet, F. Montaigne, P. Seneor, and A. Vaurès, Phys. Rev. Lett. **82**, 4288 (1999).
[49] M. Sharma, S. X. Wang, and J. H. Nickel, Phys. Rev. Lett. **82**, 616 (1999).
[50] J. Moser *et al.*, Appl. Phys. Lett. **89**, 162106 (2006).
[51] C. Heiliger, P. Zahn, B. Y. Yavorsky, and I. Mertig, Phys. Rev. B **72**, 180406(R) (2005).
[52] E. Y. Tsymbal, A. Sokolov, I. F. Sabirianov, and B. Doudin, Phys. Rev. Lett. **90**, 186602 (2003).
[53] S. C. Erwin, S.-H. Lee, and M. Scheffler, Phys. Rev. B **65**, 205422 (2002).
[54] T. J. Zega, A. T. Hanbicki, S. C. Erwin, I. Žutić, G. Kioseoglou, C. H. Li, B. T. Jonker, and R. M. Stroud, Phys. Rev. Lett. **96**, 196101 (2006).
[55] A. Matos-Abiague, M. Gmitra, and J. Fabian (unpublished).
[56] E. A. de Andrada e Silva, G. C. La Rocca, and F. Bassani, Phys. Rev. B **55**, 16293 (1997).
[57] S. LaShell, B. A. McDougall, and E. Jensen, Phys. Rev. Lett. **77**, 3419 (1996).
[58] J. Henk, M. Hoesch, J. Osterwalder, A. Ernst, and P. Bruno, J. Phys.: Condens. Matter **16**, 7581 (2004).